



Calhoun: The NPS Institutional Archive

Theses and Dissertations

Thesis Collection

2009-06

Modeling for ship power system emulation

Leghorn, Jeremy T.

Monterey, California. Naval Postgraduate School

<http://hdl.handle.net/10945/4302>



Calhoun is a project of the Dudley Knox Library at NPS, furthering the precepts and goals of open government and government transparency. All information contained herein has been approved for release by the NPS Public Affairs Officer.

Dudley Knox Library / Naval Postgraduate School
411 Dyer Road / 1 University Circle
Monterey, California USA 93943

<http://www.nps.edu/library>

Modeling for Ship Power System Emulation

by

Jeremy T. Leghorn

B.S. Electrical Engineering University of Connecticut, 1996

Submitted to the Department of Mechanical Engineering and Electrical Engineering and
Computer Science in Partial Fulfillment of the Requirements for the Degrees of

Naval Engineer

and

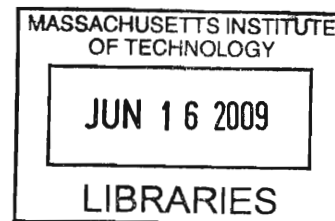
Master of Science in Electrical Engineering and Computer Science

at the

MASSACHUSETTS INSTITUTE OF TECHNOLOGY

JUNE 2009

ARCHIVE
ARCHIVES



© 2009 Jeremy T. Leghorn. All rights reserved.

The author hereby grants to MIT permission to reproduce and to distribute publicly paper and
electronic copies of this thesis document in whole or in part in any medium now known or
hereafter created.

Signature of Author

Department of Mechanical Engineering &
Electrical Engineering and Computer Science
May 8, 2009

Certified by

Steven B. Leeb
Professor of Electrical Engineering and Computer Science & Mechanical Engineering
Thesis Supervisor

Certified by

Robert W. Cox
Assistant Professor of Electrical and Computer Engineering, UNC Charlotte
Thesis Supervisor

Accepted by

Terry P. Orlando
Chairman, Department Committee on Graduate Students
MIT Department of Electrical Engineering and Computer Science

Accepted by

David E. Hardt
Chairman, Department Committee on Graduate Students
Department of Mechanical Engineering

Page Intentionally Left Blank

Modeling for Ship Power System Emulation

by

Jeremy T. Leghorn

Submitted to the Department of Mechanical Engineering
and Electrical Engineering and Computer Science
on May 8, 2009 in Partial Fulfillment of the
Requirements for the Degrees of

Naval Engineer
and
Master of Science in Electrical Engineering and Computer Science

ABSTRACT

With the U.S. Navy's continued focus on Integrated Fight Thru Power (IFTP) there has been an ever increasing effort to ensure an electrical distribution system that maintains maximum capabilities in the event of system faults. This is to ensure that the crew has the ability to complete real time tactical missions in the event of battle damage to any localized portions of the electrical distribution system. Fault isolation is a priority component of the U.S. Navy's Next Generation Integrated Power System (NGIPS) Roadmap, which lays out the framework as well as milestone dates for future development. Non-Intrusive Load Monitoring (NILM), which has been used extensively for condition based maintenance applications, could simultaneously be used to enhance the existing zonal protection system employed with Multi-Function Monitors (MFM). NILM may be able to, inexpensively, use the existing current and voltage sensors available from the MFM hardware to determine electrical loading which could allow for faster fault isolation capability.

A test platform with three 5000 watt synchronous generators is being constructed to emulate a U.S. Navy DDG 51 FLT IIA class ship electric plant. This is being accomplished in order to evaluate the feasibility of improving the fault isolation capabilities of the MFM with NILM implementation. The first step in this endeavor will be to electrically relate the test platform to the DDG electric plant. In order to accomplish this step, the fault simulation results from the test platform will be compared to simulated faults using U.S. Navy data from DDG 51 electric plants. This will allow for the fault isolation results from the test platform to be related to the DDG 51 electric plant.

Thesis Supervisor: Steven B. Leeb

Title: Professor of Electrical Engineering and Computer Science & Mechanical Engineering

Thesis Supervisor: Robert W. Cox

Title: Assistant Professor of Electrical and Computer Engineering, UNC Charlotte

Acknowledgements

The author would like to acknowledge the following individuals for their assistance. Without them this thesis would not have been possible.

- Professor Steven Leeb for providing me with a challenging and rewarding experience
- Professor Robert Cox for his enthusiasm, assistance and feedback
- Warit Wichakool for his technical expertise and willingness to help
- Uzoma Orji for his software and technical expertise and willingness to help
- Captain Norbert Doerry for providing all the information and contacts necessary to help with my thesis
- Timothy Zavertrnik for his willingness to provide data and answer questions
- Keith Douglas and Greg Elkins for their technical acumen and ability to keep things fun during shipboard installations.

Finally, thanks and love to my wife and daughter who have been patient and supportive throughout this process.

Table of Contents

Acknowledgements.....	4
Table of Contents.....	5
List of Figures.....	7
List of Tables.....	9
1.0 Introduction.....	10
1.1 Background.....	10
1.2 Non-Intrusive Load Monitor (NILM).....	12
1.3 Thesis Objectives.....	13
2.0 Zonal Electrical Distribution System with MFM III.....	15
2.1 High Speed Relay (HSR) Algorithm.....	17
3.0 Synchronous Machines.....	20
3.1 Basic Machine Layout.....	20
3.2 Direct and Quadrature Transformation.....	21
3.3 Equal Mutuals Model Description.....	25
4.0 Preliminary Data Collection.....	28
4.1 DC test.....	28
4.2 Open-Circuit Test: Magnetization Characteristic and Field Resistance.....	29
4.3 Short Circuit Characteristics.....	31
4.4 Short Circuit Testing.....	34
4.4.1 Test Setup.....	35
4.4.2 Test Results.....	37
4.4.3 Analysis of Data.....	40
5.0 Generator Modeling.....	43

5.1 Equal Mutuals Modeling.....	43
5.1.1 Bench Generator Model.....	46
5.1.2 Sensitivity Analysis.....	52
5.1.2 DDG Model.....	54
5.2 DDG and Bench Generator Comparison.....	57
5.2.1 Armature Reaction for DDG and Bench Generator.....	63
6.0 Future Studies.....	65
6.1 Additional Work.....	65
6.2 Conclusion.....	66
BIBLIOGRAPHY.....	68
APPENDIX 1 - MATLAB Evaluation of Xd.....	69
APPENDIX 2 - MATLAB tachometer to frequency code.....	73
APPENDIX 3 – MATLAB Bench Generator Model Code.....	75
APPENDIX 4 – MATLAB DDG-51 Simulation Code and DDG-II Results.....	81
APPENDIX 5 – SIMULATION USERS GUIDE.....	87
APPENDIX 6 – MATLAB MODEL VERIFICATION.....	89
APPENDIX 7 – CALCULATION OF NAVSEA DDG PARAMETERS.....	100

List of Figures

Figure 1: NILM architecture (3)	12
Figure 2: NILM installation (3).	13
Figure 3: Ming Dong 5000 Watt Bench Generator	14
Figure 4: Multi Function Module (MFM III)	16
Figure 5: Electric Plant Layout (DDG51 FLT IIA)	17
Figure 6: Four pole, Y-Connected Synchronous Generator (5).....	20
Figure 7: Direct Axis Model.....	26
Figure 8: Quadrature Axis Model.....	26
Figure 9: Bench Generator Y-configuration(7)	29
Figure 10: Bench Generator OCC.....	30
Figure 11: SCC and OCC test setup (7).....	31
Figure 12: Bench Generator I_{SCC}	32
Figure 13: Bench Generator OCC and SCC	32
Figure 14: Bench Generator D-Axis Reactance.....	33
Figure 15: Short circuit envelope (classical equation) (8).....	35
Figure 16: Bench Generator Prime Mover (1.5 HP).....	36
Figure 17: Switching Apparatus for short circuit implementation	36
Figure 18: Short Circuit Results from Oscilloscope	37
Figure 19: Field Current during short circuit.....	38
Figure 20: Speed profile for Short Circuit (Tachometer and Inertia Constant).....	39
Figure 21: Evaluation of X_d'	40
Figure 22: X_d'' Determination.....	41
Figure 23: Direct and Quadrature Axes (6)	45
Figure 24: Bench Generator Simulation	51
Figure 25: Bench Generator (Simulation, Classical, and Actual) Results	52
Figure 26: DDG-I Short Circuit (Initially Unloaded).....	56
Figure 27: DDG-I Short Circuit (Initially Fully Loaded)	56
Figure 28: Pole Zero Plots for Bench Generator and DDG-I Model.....	58
Figure 29: Impedance Bode Plots (Bench Generator and DDG-I).....	59

Figure 30: DDG-51 Current Threshold after Three Phase Fault (Initially Unloaded – Left), (Initially Fully Loaded - Right).....	60
Figure 31: Bench Generator Current Threshold (Initially Unloaded – Left), (Initially Fully Loaded - Right).....	60
Figure 32: Bench Generator Actual Phase Current Crossing 150% Threshold.....	62
Figure 33: Effect of Armature Resistance on Short Circuit Current for DDG	64
Figure 34: DDG-II Short Circuit Simulation (Initially Unloaded).....	85
Figure 35: DDG-II Short Circuit Simulation Frequency Response (Initially Unloaded).....	86
Figure 36: Krause Simulation used to verify Equal Mutuals Simulation Model.....	89
Figure 37: Krause Simulation Results	90
Figure 38: Equal Mutuals Model Results for Krause Simulation (Phase, Direct, and Quadrature Currents)	97
Figure 39: Equal Mutuals Model Results for Krause Simulation (Frequency and Degrees)	98
Figure 40: Equal Mutuals Model Results for Krause Simulation (Field Current and Torque)	99

List of Tables

Table 1: Bench Generator Specifications	28
Table 2: Bench Generator Parameters	48
Table 3: Simulation and Classical results compared to Actual Data	52
Table 4: Bench Generator Model Sensitivity Parameters (First Peak Current).....	53
Table 5: Bench Generator Sensitivity Parameters (Decay Envelope)	54
Table 6: DDG-51 generator parameters provided by NAVSEA	55
Table 7: Generator Times for Fault Detection (150% Current).....	62
Table 8: Armature time constants for DDG and Bench Generator.....	63

Chapter 1

1.0 Introduction

The DDG-51 FLT IIA class ships currently use Multi-function Monitors (MFMs) to quickly locate and isolate electrical faults. These systems perform fault detection using the high speed relay (HSR) algorithm that monitors the magnitude and phase of the various system voltages (1). One difficulty encountered when implementing the HSR algorithm is the need to be able to distinguish between true faults and momentary voltage “spikes” that occur because of switching events and other normal activities. Because most spikes dampen out quickly, they can be easily detected using additional samples or removed using low-pass filters. Both of these options add delays to the HSR algorithm, thus limiting its ability to detect true faults. Careful adjustment of the algorithm’s thresholds is necessary both to prevent voltage degradations that can disrupt power quality during faults and to avoid false alarms. As NAVSEA has found, it is difficult to determine optimal threshold settings using only laboratory test circuits. Instead, appropriate thresholds can only be determined if one knows the maximum allowable waveform distortion, and this can be different depending on the shipboard environment (2). One way to solve this problem is to integrate the MFM with a tool known as the non-intrusive load monitor (NILM). The NILM is a device that can classify various transient events in power systems, and it has been used repeatedly for load-identification in shipboard environments (3). The NILM may be able to improve the HSR performance by identifying switching events and by maintaining a list of currently operating loads. With this information, it becomes possible to dynamically select settings based on current conditions.

1.1 Background

With the US Navy warships evolution to the Integrated Power Systems (IPS) architecture an emphasis has been placed on Zonal Electrical Distribution Systems (ZEDS). ZEDS focus on classifying electrical loads into three categories (uninterruptible, short term interrupt, and long term interrupt) (4). Uninterruptible loads would include items such as that necessary to execute

the ships mission (including weaponry, sensors, communication, and propulsion systems). IPS will provide electric propulsion and ship service electrical loads, from a common power source, into one distribution system. Historically this has not been the case. Propulsion requirements have been achieved mechanically through either a diesel or gas turbine coupled to a shaft through an intermediary reduction gear. This in turn has buffered the propulsion plant from having any direct degradation effects as a result of most electric plant casualties. Electric plants have been maintained in redundant split bus configurations as well as having separate vital and non-vital busses. The vital busses would contain items necessary for war fighting as well as equipment necessary for maintaining propulsion such as propulsion lube oil. In the event of casualties, the plant has been designed to maximize continuity of power to the vital bus while also ensuring that the non-vital bus is the first to be disconnected. This has been accomplished by having breakers that open on such items as over-current, under-frequency, over-frequency, under-voltage, along with other very specific criteria. Electric plants have not been designed to logically assess where a fault is coming from and to only isolate power locally to those affected areas. However, with the advent of electric propulsion it is now necessary to be able to localize and isolate faults to only those zones affected in order to ensure maximized propulsion capabilities as well as war fighting capabilities. This is known as Integrated Fight Through Power (IFTP) and is accomplished by having a ZEDS that uses Multi-Function Monitors (MFM) and a High Speed Relay (HSR) algorithm. The MFM is used to identify where faults are originating and to only isolate those areas. Currently MFM III operation requires a fault threshold to be set which will discriminate faults from typical plant transients. The plant transients must be assessed for the worst case loading scenarios which could delay true fault responses. Information obtained from NILM could potentially be used to optimize fault thresholds based on current plant loading.

The Next Generation Integrated Power System (NGIPS) has listed as challenges for future implementation of AC ZEDS the implementation of mission priority load shedding. NILM could aid this process by having knowledge of current power loading as well as the capability of knowing which loads are currently operating real time. Through this knowledge NILM could communicate the need to turn off non-vital loads when power is mission limiting.

The NGIPS description of what is desired in Power Control Modules (PCON) leads to a conclusion that NILM could be developed to meet those requirements. The primary functions of PCON which could be improved by NILM are the following (4):

1. Remote monitoring and control of NGIPS modules.
2. Mission priority load shedding.
3. Fault detection and isolation.
4. Maintenance support.

1.2 Non-Intrusive Load Monitor (NILM)

The NILM is a device that measures at least one voltage, and one line current with a transducer at a particular point in an electrical distribution system. These measurements are used to calculate both real and reactive power envelopes as well as harmonic frequency content. These measurements and calculated values can be used for monitoring which loads are currently operating and in what mode (e.g. slow speed or fast speed pumps), as well as for determining if equipment is operating correctly or is need of maintenance. NILM can be used for power monitoring and evaluation of fault conditions in conjunction with MFM and HSR algorithms.

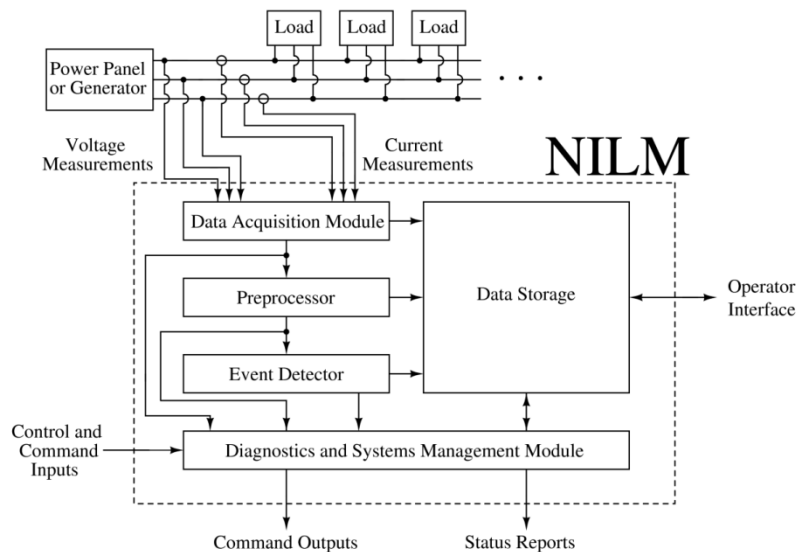


Figure 1: NILM architecture (3)

The NILM architecture is shown in Figure 1. It allows for command and control inputs, operator interface, command outputs, and status reports. An interface would need to be developed for NILM and MFM to operate together. This could be developed within the current NILM architecture. A typical installation, as installed on the Famous Class USCG Cutter (WMEC-907 Escanaba), is shown in Figure 2.

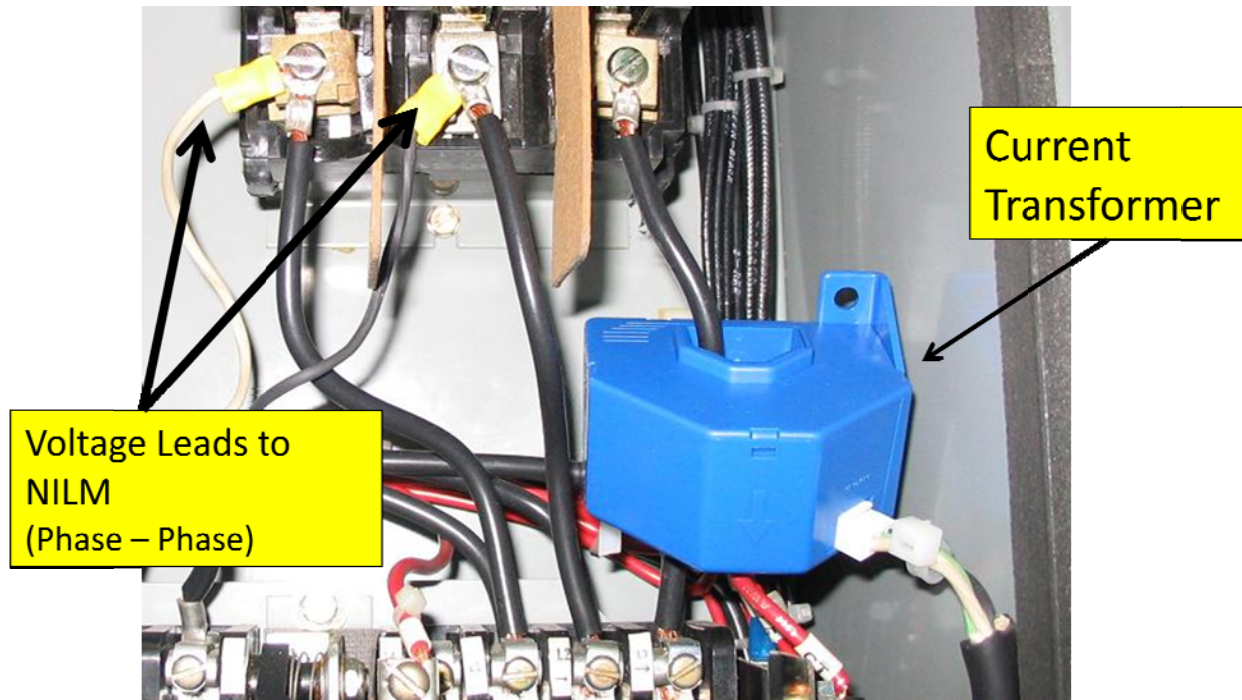


Figure 2: NILM installation (3).

The NILM, to date, has been used in radial distribution systems and has not been explored in a ring distribution system such as that employed by DDG IIA. An important reason for building the hardware emulator is to test NILM capabilities in a ring distribution plant.

1.3 Thesis Objectives

The 5000 Watt bench generator shown in Figure 3 is being electrically and mechanically characterized to determine feasibility as a test platform for NILM fault studies. The purpose of

this thesis is to compare the characteristics of the bench generator to a DDG-51 gas turbine generator. The first step for this project is to obtain short circuit real data for the bench generator and then to match a simulation to the real data. When this is accomplished it means that the short circuit time constants as well as the transient reactances are known and the response of the bench generator can be predicted for fault conditions. NAVSEA has provided data necessary to simulate short circuits for DDG-51 gas turbine generators associated with 3 MW and 4.5 MW plants. Since the reactances and time constants for the bench generator and DDG-51 plants are known they can be used to scale and compare the NILM bench generator results to a potential realization of NILM implementation on a DDG-51 plant. These results would need to be confirmed in an actual DDG-51 plant and the goal would be to do so at the Land Based Engineering Site (LBES) in Philadelphia, PA.

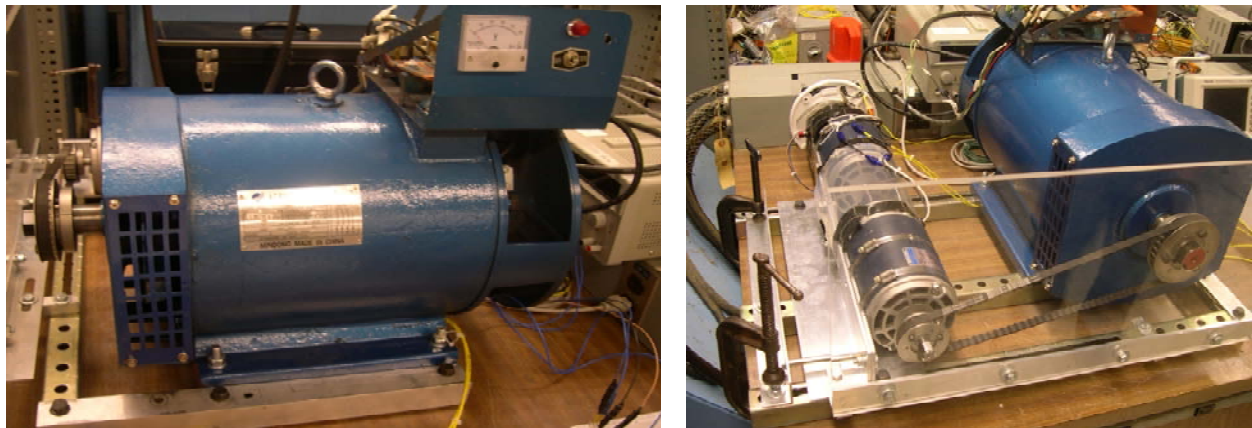


Figure 3: Ming Dong 5000 Watt Bench Generator

The bench generator is a 4 pole, field wound synchronous generator. The stator is Y-connected with the neutral ungrounded and a rated voltage of $120 V_{RMS}$ phase to neutral. Characterization of the generator parameters are discussed in chapter 5. The bench generator is being driven by a 1.5 HP DC motor (120 Volts DC, 11.2 Amps, 4800 RPM). Feedback loops are being used to control armature frequency and voltage responses. The goal is to relate the speed and voltage responses of the bench generator to a DDG-51 plant response.

Chapter 2

The DDG IIA electric plant was developed in accordance with the NGIPS architecture for zonal electrical distribution systems. The DDG IIA plant is a ring distribution system which means that power flowing to a particular load may be coming from more than one generator. Having a NILM located at each MFM will place it upstream in the electric plant such that the power flowing to a particular load may be going through more than one NILM. Chapter 1 discussed that classifying the bench generator, both mechanically and electrically, is the first step towards the final goal of having a hardware emulator for the DDG IIA electric plant. One of the major reasons for the hardware emulator is to test the NILM in a ring distribution lineup to evaluate if power to particular loads may be seen from more than one NILM. The ability to identify loads in a ring distribution plant could potentially be used by MFM to improve fault localization times. This chapter will provide information about the DDG IIA plant and MFM to show the motivation for the hardware emulator realization.

2.0 Zonal Electrical Distribution System with MFM III

Figure 4 below shows the MFM currently employed on DDG-51 FLT IIA plants. The unit is responsible for the following actions (1):

1. Importing voltage, current, and circuit breaker status.
2. Processing voltage and current data to detect fault conditions.
3. Communicate with the other MFM throughout the plant.
4. Make shunt trip decisions.

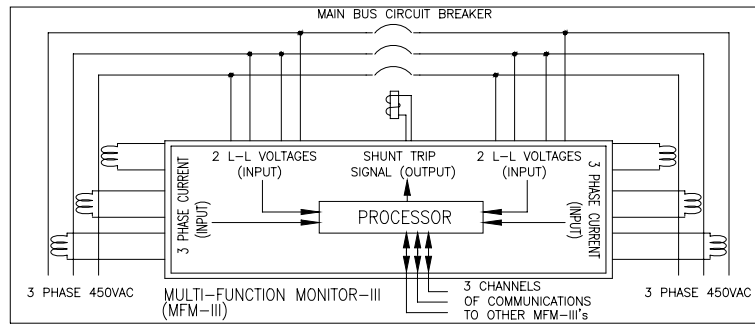


Figure 4: Multi Function Module (MFM III)

The MFM III unit monitors two channels of data associated with each circuit breaker. The channels correspond to information on the upstream and downstream sides of the circuit breaker. Each channel has two voltage sensors that monitor phase-to-phase voltages (V_{ab} , V_{cb}) from potential transformers (440:110), as well as all three line currents from current transformers (6000:5). The MFM units also have three ethernet communication ports that are used for point to point communications as well as “ring” communications. All of the MFM modules are in direct communications with the MFM that are adjacent to them. This is referred to as point to point communications. These communications are necessary because trip logic for isolation determination is dependent on the status of adjacent circuit breakers. The MFM point to point communications occur every 1.0 ms. Ring communications are system wide. Every 5.0 ms the ring communication network sends out information with a status of all MFM to all units. A shunt trip signal is generated based on each MFM local voltage and current measurements as well as logic tables associated with the other MFM in the system. The plant configuration for the DDG-51 FLT IIA is shown in Figure 5.

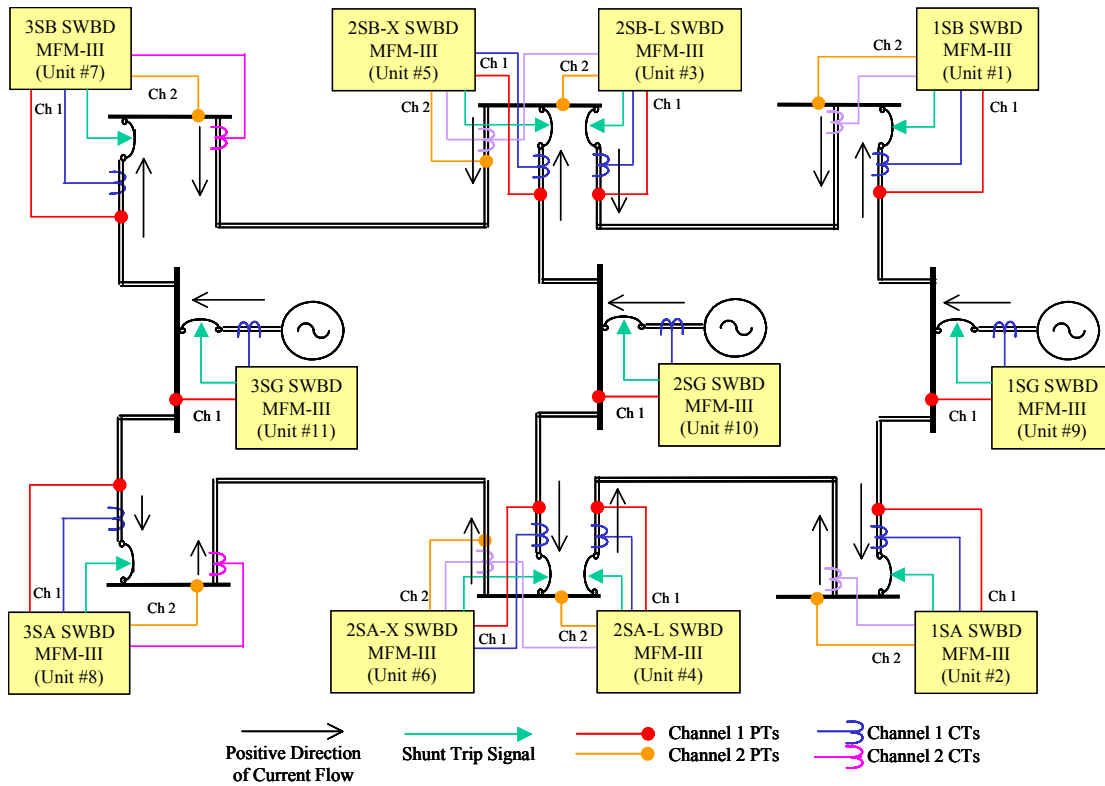


Figure 5: Electric Plant Layout (DDG51 FLT IIA)

Since both MFM and NILM monitor phase-to-phase voltages and line currents there is an opportunity to have both systems collocated and operating from the same set of inputs. NILM capabilities could enhance MFM III operation through optimization of trip set points as well as adding the proven benefits of equipment monitoring for conditions based maintenance.

2.1 High Speed Relay (HSR) Algorithm

MFM uses the HSR algorithm to assess when fault conditions occur and to determine where the fault is occurring such that the electric distribution system only isolates those affected areas. The algorithm uses the infamous Parks transformation of the three phase voltages to discriminate faults from normal ships transients and uses changes in power flow to assess where a fault is located. Figure 5 above shows what the positive direction of current flow which is the same as positive power flow. The Park transformation is shown below.

$$\begin{bmatrix} v_0 \\ v_d \\ v_q \end{bmatrix} = \sqrt{\frac{2}{3}} \begin{bmatrix} \frac{1}{\sqrt{2}} & \frac{1}{\sqrt{2}} & \frac{1}{\sqrt{2}} \\ \cos \omega t & \cos\left(\omega t - \frac{2\pi}{3}\right) & \cos\left(\omega t + \frac{2\pi}{3}\right) \\ \sin \omega t & \sin\left(\omega t - \frac{2\pi}{3}\right) & \sin\left(\omega t + \frac{2\pi}{3}\right) \end{bmatrix} \begin{bmatrix} v_a \\ v_b \\ v_c \end{bmatrix}$$

Where the voltage, v , is transformed from the rotating reference frame of a, b, and c to the direct and quadrature frame of reference of d and q. If the sum of v_a , v_b , and v_c are equal to zero than v_0 will also equal zero which is the assumption used in the HSR algorithm. The assumption of a constant operating frequency results in the time varying functions of voltage being transformed into a constant magnitude and angle as shown below.

$$\begin{aligned} v_a &= V_a \cos(\omega t + \varphi) \\ v_b &= V_b \cos\left(\omega t - \frac{2\pi}{3} + \varphi\right) \\ v_c &= V_c \cos\left(\omega t + \frac{2\pi}{3} + \varphi\right) \\ V_{dq} &= \left| \sqrt{\frac{3}{2}} V \right|, < -\varphi \end{aligned}$$

The magnitude and phase of V_{dq} can then be used to assess whether a fault condition has occurred. In normal plant operations, with changing load conditions, there will be changes in V_{dq} but these will be a small percent of what would be seen in a fault condition. Any changes in magnitude by a set threshold $\pm(T_M)$ between successive samples would be assessed as a fault condition. Similarly, any changes in angle, φ , would indicate changes in synchronization and would be compared to thresholds established to determine fault conditions.

Once a fault has been detected the HSR algorithm then uses a running average of power to determine the direction of the fault with respect to each individual MFM. These directions are with respect to the direction of current flow as shown schematically in Figure 5. Once a fault has been identified, through use of the Parks transformation on phase-to-phase voltages, power is assessed to determine which breakers need to be tripped. At each MFM power is calculated for

each sample and a running average is kept. After a fault condition is assessed the average value of power, at each MFM, is frozen and used to compare to successive power calculations during the fault. If power increases by a factor of 1.5 over the steady state average power at a particular MFM, the associated circuit breaker gets tripped. Power is calculated according to calculations shown below.

$$\begin{aligned}
 \text{Power} &= v_{an}i_a + v_{bn}i_b + v_{cn}i_c \\
 &= v_{an}i_a + v_{bn}i_b + v_{cn}i_c + v_{cn}(i_a - i_a) + v_{cn}(i_b - i_b) \\
 &= (v_{an} - v_{cn})i_a + (v_{bn} - v_{cn})i_b + v_{cn}(i_a + i_b + i_c) \\
 &= -v_{ca}i_a + v_{bc}i_b + v_{cn}(i_a + i_b + i_c) \\
 &\cong -v_{ca}i_a + v_{bc}i_b
 \end{aligned}$$

The power equation is derived above to use the actual inputs that are provided from the MFM which are the two phases-to-phase voltages and three line currents. It is observed that this still requires a line to neutral voltage, v_{cn} , which the MFM does not provide. Once again the assumption is that the three line currents will sum to zero in which case the line to neutral voltage is not needed. If the sum of the currents are not zero than the power calculated is not correct. This is because the fault can no longer be modeled as a load on that particular line and involves a connection to another point in the system (2). In this case more than one MFM would activate a shunt trip in order to fully isolate the fault.

Chapter 3

The previous chapters have discussed the motivation for building an emulator for the DDG IIA plant. The first step towards building an emulator is to characterize the bench generator that will be used. To accomplish this, laboratory experiments will be conducted to derive electrical constants. Once identified, the electrical constants can be used to simulate the bench generator. This chapter will discuss the background of the electrical generator that is being evaluated for use in the hardware emulator. Also discussed is the simulation that will be used for the bench generator and the DDG generator.

3.0 Synchronous Machines

3.1 Basic Machine Layout

Shown in Figure 6 is a three phase, four pole, Y-connected synchronous generator. The bench generator is a salient poled generator. The armature winding is on the stator and the field winding is on the rotor. The field winding is excited by a DC voltage source which is applied

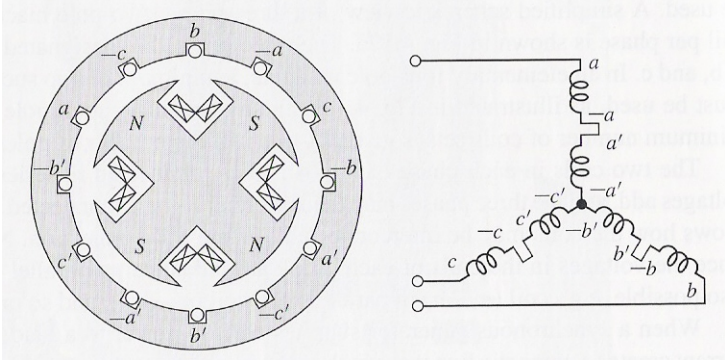


Figure 6: Four pole, Y-Connected Synchronous Generator (5)

through a set of stationary brushes which are in contact with rotating slip rings. Since the generator has two sets of poles, every time the rotor rotates one full revolution the generator electrical frequency rotates two full revolutions. This results in the generator having an electrical

frequency of 60 Hz when the mechanical frequency, n , of the generator is 1800 RPM as shown in the equation below.

$$f_e = \left(\frac{\text{poles}}{2} \right) \frac{n}{60} \text{ Hz}$$

3.2 Direct and Quadrature Transformation

The synchronous generator can be represented by 6 windings. The windings are the three armature windings, the field winding, and two damper windings (one on the direct axis of the field winding and the other on the quadrature axis). The equations representing the synchronous machine are as shown below (6).

$$\begin{bmatrix} \underline{\lambda}_{ph} \\ \underline{\lambda}_R \end{bmatrix} = \begin{bmatrix} \underline{L}_{ph} & \underline{M} \\ \underline{M}^T & \underline{L}_R \end{bmatrix} \begin{bmatrix} \underline{I}_{ph} \\ \underline{I}_R \end{bmatrix}$$

Where,

$$\underline{\lambda}_{ph} = \begin{bmatrix} \lambda_a \\ \lambda_b \\ \lambda_c \end{bmatrix} \quad \underline{\lambda}_R = \begin{bmatrix} \lambda_f \\ \lambda_{kd} \\ \lambda_{kq} \end{bmatrix} \quad \underline{I}_{ph} = \begin{bmatrix} I_a \\ I_b \\ I_c \end{bmatrix} \quad \underline{I}_R = \begin{bmatrix} I_f \\ I_{kd} \\ I_{kq} \end{bmatrix}$$

and,

$$\underline{L}_{ph} = \begin{bmatrix} L_a & L_{ab} & L_{ac} \\ L_{ab} & L_b & L_{bc} \\ L_{ac} & L_{bc} & L_c \end{bmatrix} \quad \underline{L}_R = \begin{bmatrix} L_f & L_{fkd} & 0 \\ L_{fkd} & L_{kd} & 0 \\ 0 & 0 & L_{kq} \end{bmatrix}$$

From these equations it can be seen that the direct axis rotor flux is not dependent on the quadrature damping currents. The same is true that the quadrature axis flux does not depend on the field current or the direct axis damping current.

$$\underline{\underline{M}} = \begin{bmatrix} M \cos \theta & L_{akd} \cos \theta & -L_{akq} \sin \theta \\ M \cos \left(\theta - \frac{2\pi}{3} \right) & L_{akd} \cos \left(\theta - \frac{2\pi}{3} \right) & -L_{akq} \sin \left(\theta - \frac{2\pi}{3} \right) \\ M \cos \left(\theta + \frac{2\pi}{3} \right) & L_{akd} \cos \left(\theta + \frac{2\pi}{3} \right) & -L_{akq} \sin \left(\theta + \frac{2\pi}{3} \right) \end{bmatrix}$$

The stator to rotor mutual inductance ($\underline{\underline{M}}$) relates the phase fluxes to the rotor currents and the rotor fluxes to the phase currents. The stator to rotor mutual inductance is dependent on the angle of the rotor to the line of flux aligned with the phase A current and as such will have a time dependency as the rotor rotates.

$$\begin{aligned} L_a &= L_{a0} + L_2 \cos 2(\theta) \\ L_b &= L_{a0} + L_2 \cos 2 \left(\theta - \frac{2\pi}{3} \right) \\ L_c &= L_{a0} + L_2 \cos 2 \left(\theta + \frac{2\pi}{3} \right) \\ L_{ab} &= L_{ab0} + L_2 \cos 2 \left(\theta - \frac{\pi}{3} \right) \\ L_{bc} &= L_{ab0} + L_2 \cos 2(\theta) \\ L_{ac} &= L_{ab0} + L_2 \cos 2 \left(\theta + \frac{\pi}{3} \right) \end{aligned}$$

For the bench generator there is saliency which explains the form of the equations above for L_a , L_b , L_c , L_{ab} , L_{bc} , and L_{ac} . L_2 is the same in each of the expressions and θ is the position of the rotor relative to phase A. The Parks transformation will be used to transform to a coordinate system in which the rotor is stationary. For the proof shown below $\underline{\underline{T}}$ is the Parks transformation and $\underline{\underline{T}}^{-1}$ is the inverse Parks transformation.

$$\underline{\lambda}_{ph} = \underline{\underline{L}}_{ph} \underline{I}_{ph} + \underline{\underline{M}} \underline{I}_R$$

Now apply the Parks transformation. In the equation below we set $\underline{I}_{ph} = \underline{\underline{T}}^{-1} \underline{I}_{dq}$.

$$\underline{\underline{T}} \underline{\underline{\lambda}}_{ph} = \underline{\underline{T}} \underline{\underline{L}}_{ph} \underline{\underline{T}}^{-1} \underline{\underline{I}}_{dq} + \underline{\underline{T}} \underline{\underline{M}} \underline{\underline{I}}_R$$

Since $\underline{\underline{T}} \underline{\underline{\lambda}}_{ph} = \underline{\underline{\lambda}}_{dq}$, we can rewrite the equation as shown below.

$$\underline{\underline{\lambda}}_{dq} = \underline{\underline{L}}_{dq} \underline{\underline{I}}_{dq} + \underline{\underline{L}}_C \underline{\underline{I}}_R$$

Where,

$$\underline{\underline{L}}_{dq} = \underline{\underline{T}} \underline{\underline{L}}_{ph} \underline{\underline{T}}^{-1}$$

$$\underline{\underline{L}}_C = \underline{\underline{T}} \underline{\underline{M}}$$

Using the same methodology one can obtain the following equations for the rotor fluxes.

$$\begin{aligned} \underline{\underline{\lambda}}_R &= \underline{\underline{M}}^T \underline{\underline{T}}^{-1} \underline{\underline{I}}_{dq} + \underline{\underline{L}}_R \underline{\underline{I}}_R \\ &= \frac{3}{2} \underline{\underline{L}}_C^T \underline{\underline{I}}_{dq} + \underline{\underline{L}}_R \underline{\underline{I}}_R \end{aligned}$$

Where,

$$\frac{3}{2} \underline{\underline{L}}_C^T = \underline{\underline{M}}^T \underline{\underline{T}}^{-1}$$

Putting it altogether in one equation we have,

$$\begin{bmatrix} \underline{\underline{\lambda}}_{dq} \\ \underline{\underline{\lambda}}_R \end{bmatrix} = \begin{bmatrix} \underline{\underline{L}}_{dq} & \underline{\underline{L}}_C \\ \frac{3}{2} \underline{\underline{L}}_C^T & \underline{\underline{L}}_{ph} \end{bmatrix} \begin{bmatrix} \underline{\underline{I}}_{dq} \\ \underline{\underline{I}}_R \end{bmatrix}$$

L_{dq} and L_C have the convenient expressions shown below (6).

$$\underline{\underline{L}}_{dq} = \begin{bmatrix} L_d & 0 & 0 \\ 0 & L_q & 0 \\ 0 & 0 & L_0 \end{bmatrix} \quad \underline{\underline{L}}_C = \begin{bmatrix} M & L_{akd} & 0 \\ 0 & 0 & L_{akq} \\ 0 & 0 & 0 \end{bmatrix}$$

This is then separated into three current flux relationships for the direct axis, indirect axis, and zero sequence components. This can be accomplished because these axes are orthogonal in space (6). The zero sequence component is neglected and the direct and quadrature relationships are shown below. The zero sequence component can be neglected because any coupling to the direct axis is through higher harmonics that do not couple well to the armature (6).

$$\begin{bmatrix} \lambda_d \\ \lambda_{kd} \\ \lambda_f \end{bmatrix} = \begin{bmatrix} L_d & L_{akd} & M \\ \frac{3}{2}L_{akd} & L_{kd} & L_{fkd} \\ \frac{3}{2}M & L_{fkd} & L_f \end{bmatrix} \begin{bmatrix} I_d \\ I_{kd} \\ I_f \end{bmatrix} \quad \begin{bmatrix} \lambda_q \\ \lambda_{kq} \end{bmatrix} = \begin{bmatrix} L_q & L_{akq} \\ \frac{3}{2}L_{akq} & L_{kq} \end{bmatrix} \begin{bmatrix} I_q \\ I_{kq} \end{bmatrix}$$

Equation 1: Direct and Quadrature Flux Current Relationship

Now the above results can be used to solve for the direct and quadrature voltages.

$$\underline{V}_{ph} = \frac{d}{dt} \lambda_{ph} = \frac{d}{dt} \underline{T}^{-1} \lambda_{dq}$$

Therefore,

$$\begin{aligned} \underline{V}_{dq} &= \underline{T} \underline{V}_{ph} \\ &= \underline{T} \frac{d}{dt} (\underline{T}^{-1} \lambda_{dq}) \\ &= \frac{d}{dt} \lambda_{dq} + \left(\underline{T} \frac{d}{dt} \underline{T}^{-1} \right) \lambda_{dq} \end{aligned}$$

Where,

$$\underline{T} \frac{d}{dt} \underline{T}^{-1} = \begin{bmatrix} 0 & -\frac{d\theta}{dt} & 0 \\ \frac{d\theta}{dt} & 0 & 0 \\ 0 & 0 & 0 \end{bmatrix}$$

Which results in the final equation for direct and quadrature voltages shown below.

$$V_d = \frac{d\lambda_d}{dt} - \omega \lambda_q$$

$$V_q = \frac{d\lambda_q}{dt} - \omega\lambda_d$$

It should be noted that the voltages listed above do not include the effects of the armature resistance. To obtain the terminal voltage the armature resistance would need to be accounted for which will be shown in the next section.

3.3 Equal Mutuals Model Description

Equation 1, derived in the previous section, is an equation in which the inductance matrix has six variables. These six variables are unknown for the bench generator. The equal mutuals model is a model that sets the off diagonal terms equal to each other which allows a circuit model to be determined(6). From this simplification it is possible to determine the characteristics of the bench generator that will allow a simulation to be developed.

Equation 1 in the previous section will now be written in per unit form as shown below. A direct comparison of the electrical parameters of the DDG and bench generator is difficult since the machine ratings are different. Per unit values will be used to allow a direct comparison of the electrical constants for the bench and DDG generators.

$$\begin{bmatrix} \psi_d \\ \psi_{kd} \\ \psi_f \end{bmatrix} = \begin{bmatrix} x_d & x_{akd} & x_{ad} \\ x_{akd} & x_{kd} & x_{fkd} \\ x_{ad} & x_{fkd} & x_f \end{bmatrix} \begin{bmatrix} i_d \\ i_{kd} \\ i_f \end{bmatrix} \quad \begin{bmatrix} \psi_q \\ \psi_{kq} \end{bmatrix} = \begin{bmatrix} x_q & x_{akq} \\ x_{akq} & x_{kq} \end{bmatrix} \begin{bmatrix} i_q \\ i_{kq} \end{bmatrix}$$

The bases have been chosen such that the inductance matrices are symmetric (6). The “equal mutuals” model will now be used to set the field and damper base impedances such that all three mutual inductances are equal (6).

$$x_{akd} = x_{fkd} = x_{ad}$$

$$x_{aq} = x_{akq}$$

Where x_{akq} is now to be referred to as x_{aq} so that the quadrature model is consistent with the direct axis model.

$$\begin{bmatrix} \psi_d \\ \psi_{kd} \\ \psi_f \end{bmatrix} = \begin{bmatrix} x_d & x_{ad} & x_{ad} \\ x_{ad} & x_{kd} & x_{ad} \\ x_{ad} & x_{ad} & x_f \end{bmatrix} \begin{bmatrix} i_d \\ i_{kd} \\ i_f \end{bmatrix} \qquad \begin{bmatrix} \psi_q \\ \psi_{kq} \end{bmatrix} = \begin{bmatrix} x_q & x_{aq} \\ x_{aq} & x_{kq} \end{bmatrix} \begin{bmatrix} i_q \\ i_{kq} \end{bmatrix}$$

Equation 2: Equal Mutual Model Equations

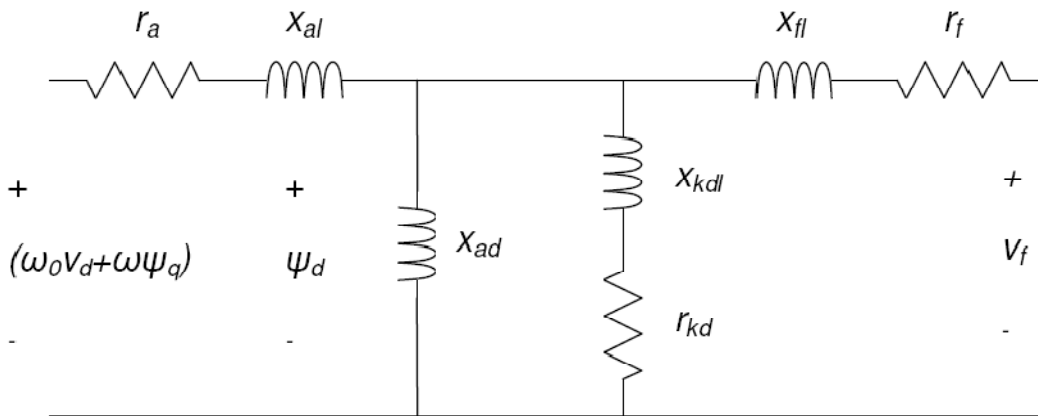


Figure 7: Direct Axis Model

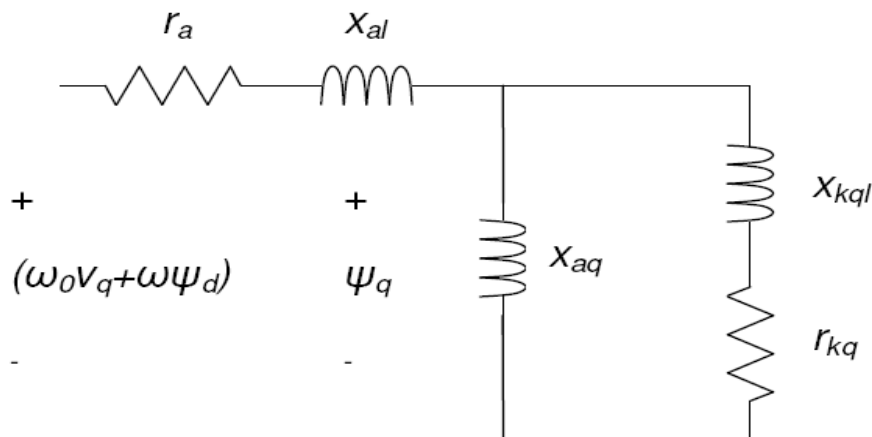


Figure 8: Quadrature Axis Model

Figure 7 and Figure 8 above show the physical model associated with Equation 2 with the leakage reactances defined as follows. (6)

$$x_{al} = x_d - x_{ad}$$

$$x_{kdl} = x_{kd} - x_{ad}$$

$$x_{fl} = x_f - x_{ad}$$

With this model the same problem as before exists which is how to obtain the relevant parameters to be able to evaluate the synchronous generator. This is discussed in chapter five but it turns out that results from short circuit testing and modeling can be used to obtain the generator parameters.

Chapter 4

This chapter will discuss all of the laboratory testing and results from the bench generator.

4.0 Preliminary Data Collection

To be able to compare the bench generators to any Navy electrical generator it is first necessary to classify the characteristics of the bench generator. The preliminary tests accomplished in order to characterize the bench generator were the following:

1. DC test: Armature Resistance (R_1). (7)
2. Open Circuit Test: The Magnetization Characteristic and Field Resistance. (7)
3. Short Circuit Test: Synchronous D-Axis Reactance (X_d). (7)

The specifications of the bench generator are shown below in Table 1. This generator is a salient pole synchronous wound field machine.

Power (W)	5000
Voltage (phase to phase), (V_{RMS})	207.85
Current (phase to neutral), (A_{RMS})	13.89
Frequency (Hz)	60
Poles	4
Power factor	0.8

Table 1: Bench Generator Specifications

4.1 DC test

The bench generator is a Y-connected generator, with the neutral ungrounded, as pictured below in Figure 9. As a result the armature resistance (R_1) is obtained simply by averaging the three armature resistances (R_a , R_b , and R_c) and multiplying by temperature and AC skin effect

correction factors (K_{TEMP} and K_{ac}). A typical value for K_{TEMP} multiplied by K_{AC} is 1.5 (7). Lab measurements yielded an armature resistance equal to 0.48Ω .

$$R_{dc} = \frac{R_{ab} + R_{bc} + R_{ca}}{6}$$

Now to account for temperature and the AC skin effect R_{dc} is multiplied by 1.5.

$$R_1 = K_{TEMP}K_{ac}R_{dc}$$

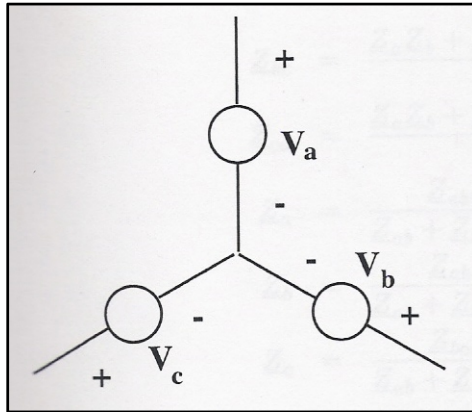


Figure 9: Bench Generator Y-configuration(7)

4.2 Open-Circuit Test: Magnetization Characteristic and Field Resistance

The Open Circuit Characteristics (OCC) are obtained with the generator at synchronous speed by measuring the open circuited armature phase to phase voltage ($E_{\phi\phi}$) while the field current (I_F) is varied such that the terminal voltage goes from zero to rated voltage. While I_F is being adjusted the field voltage (V_F) is also being measured and therefore the field resistance ($R_F = V_F/I_F$) can be averaged throughout the range of operation. The average R_F was equal to 15.8Ω .

Using the equation shown below and the open circuit characteristics lab results we can evaluate K_{ag} , A_x , and B_x .

$$I_F = \frac{E_f}{K_{ag}} + A_x e^{B_x E_f}$$

Where A_x is the change in field current which accounts for saturation, B_x is an exponential constant that determinations the exponential shape of the field current, and K_{ag} slope of the air gap line (linear portion of curve).

The results are shown below in Figure 10. The results were as expected and we see the stator voltage beginning to saturate as I_f is increased.

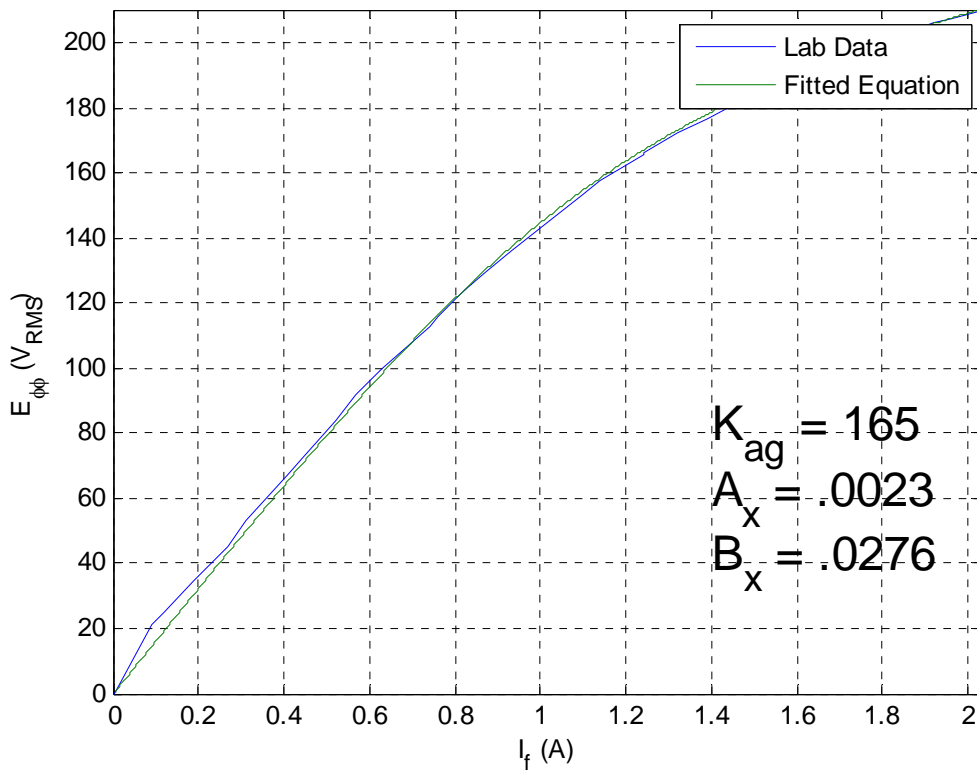


Figure 10: Bench Generator OCC

4.3 Short Circuit Characteristics

The OCC results from the previous section along with the short circuit characteristics (SCC), which will be determined in this section, will be used to determine the direct axis reactance. Using the setup shown in Figure 11 the synchronous generator was operated at rated frequency while the stator terminals were short circuited. I_F was slowly adjusted from zero amps up to 741 mA while the I_A was measured. I_a and I_F shown in Figure 11 are meters used to measure the field and stator currents.

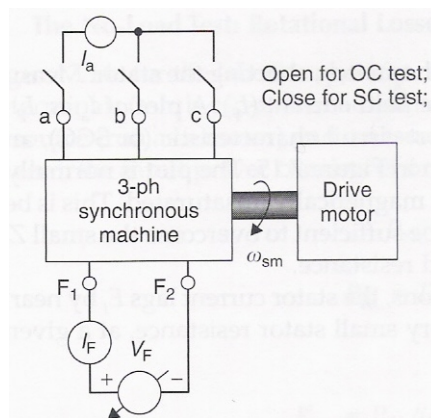


Figure 11: SCC and OCC test setup (7)

The results, called the short circuit characteristics (SCC), are linear since the air-gap flux is low and the stator is magnetically unsaturated at low levels of I_F . The results are shown in Figure 12 and Figure 13.

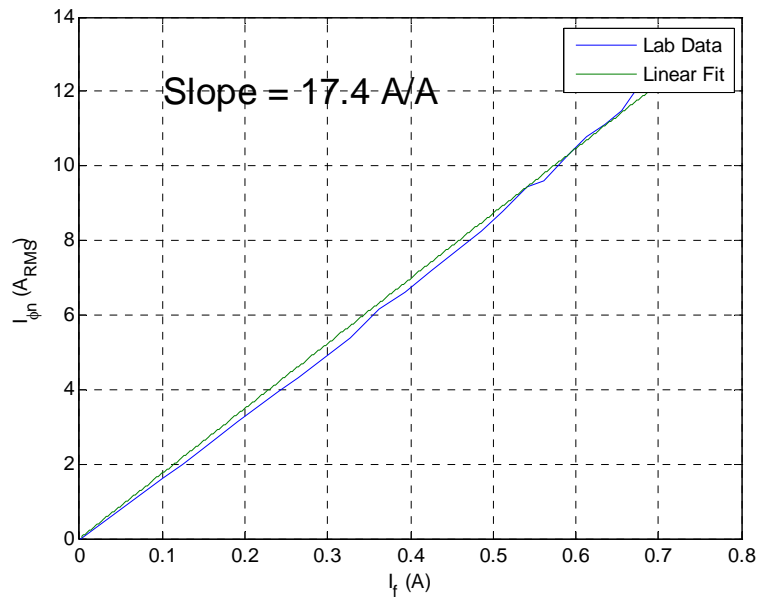


Figure 12: Bench Generator I_{sc}

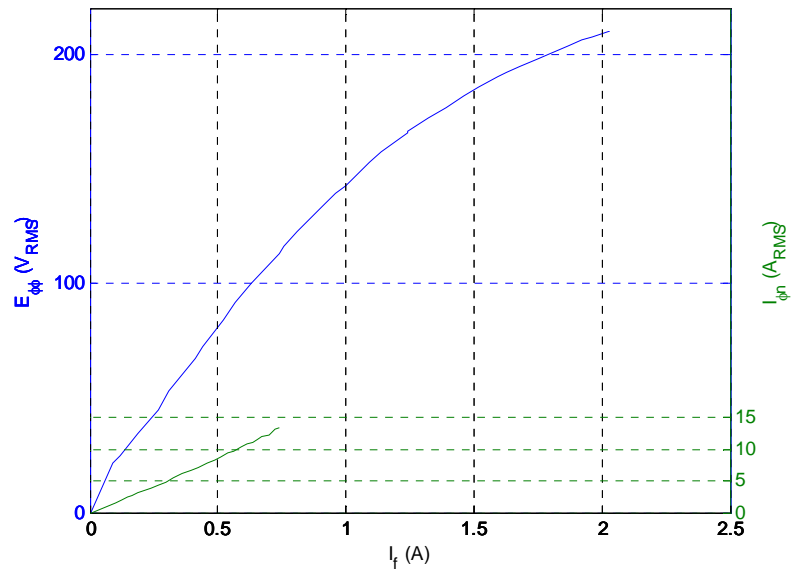


Figure 13: Bench Generator OCC and SCC

The next step in the process is taking the OCC and SCC and obtaining the d-axis reactance. Under short circuit conditions, the stator current lags the armature voltage by nearly 90° which results in I_A being approximately 100% I_d . Therefore, X_d is obtained by the following equation:

$$X_d = \frac{E_f(I_F = I_{F0}) \text{ from OCC}}{I_a(I_F = I_{F0}) \text{ from SCC}}$$

$$I_{F0} = I_F(I_a = 13.89A) \text{ from SCC} = 741mA$$

One can see that when I_F is relatively small that the armature voltage will be approximately linear. The air gap reactance X_{dag} is defined for small levels of I_F and is relatively constant. However, as the stator becomes saturated X_d will begin to decrease. The variable X_d is defined as that value of reactance that corresponds to rated armature current in Figure 13 above and as seen in Figure 14 below corresponds to 8.7Ω .

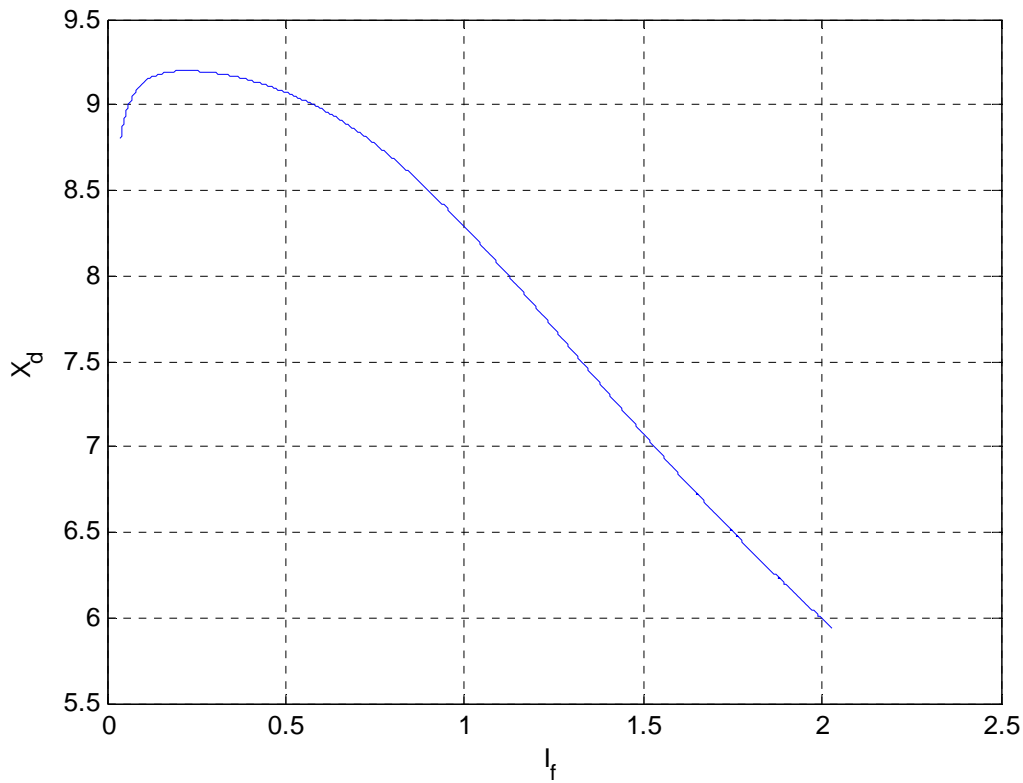


Figure 14: Bench Generator D-Axis Reactance

4.4 Short Circuit Testing

The short circuit test requires the bench generator to be operating at rated frequency and voltage open circuited. A switch is then used to short the three armature terminals simultaneously. This is not to be confused with the SCC testing that was accomplished in the previous section. The parameters that are obtained from this test are the transient and sub-transient short circuit d-axis time constants (T'_d and T''_d) as well as the transient and sub-transient d-axis reactances (X'_d and X''_d). The method employed to determine the constants was to use the equation shown below which is called the “classical short circuit” equation(8).

$$\sqrt{2}|E_a(0)| \left[\frac{1}{X_d} + \left(\frac{1}{X'_d} - \frac{1}{X_d} \right) e^{-t/T'_d} + \left(\frac{1}{X''_d} - \frac{1}{X'_d} \right) e^{-t/T''_d} \right] \sin(\omega_0 t + \delta)$$

Equation 3: Classical Short Circuit Equation

Where $E_a(0)$ is the line to neutral rated voltage which is 120 V for the generator and the sinusoidal term can correspond to any of the three phases. The importance of this equation is the exponential envelope. There are four degrees of freedom in this equation (X'_d , X''_d , T'_d , and T''_d) so an assumption is necessary to obtain the machine data. The assumption that was used was that the dominant reaction, in fact maybe the only reaction, would be as a result of the transient parameters. At the start of testing for the 5000 Watt generator there was no initial premise that any sub-transient reaction would be seen after looking at the short circuit data.

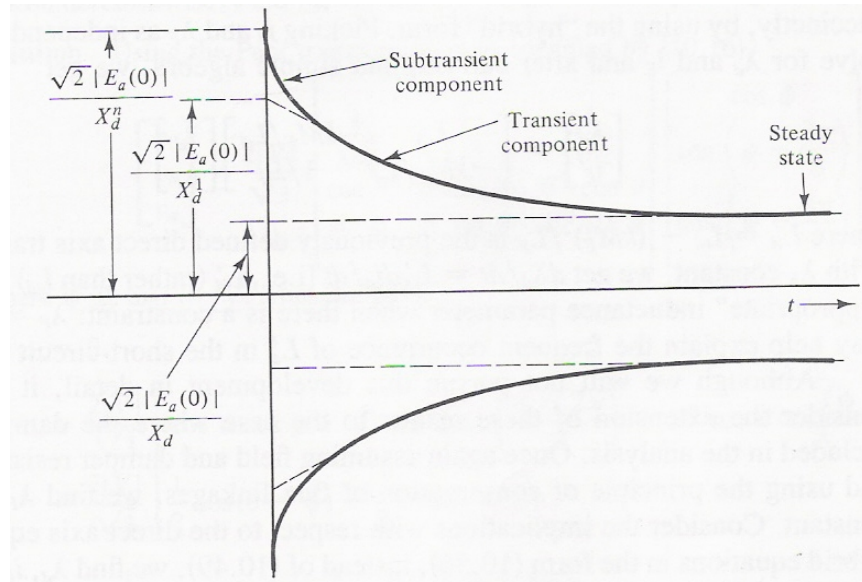


Figure 15: Short circuit envelope (classical equation) (8)

Figure 15 above shows three regions of short circuit current. The first region is the sub-transient region and the envelope is defined by X_d'' and T_d'' . The second region is the transient region and is defined by X_d' and T_d' . Finally, steady state is purely a function of the d-axis reactance (X_d). By matching the short circuit currents obtained with laboratory testing it is possible to determine all short circuit reactances and time constants.

4.4.1 Test Setup

The DC motor shown in Figure 16 was used for the initial testing of the generator. The motor is only 1.5 HP which would equal 1119 Watts of electrical power. The DC motor would not be appropriate to be the prime mover for the bench generator if we were operating under full load conditions but for purposes of obtaining constants for the generator it was an adequate motor.



Figure 16: Bench Generator Prime Mover (1.5 HP)

The motor could easily maintain the generator at 60 Hz but slowed down excessively during any loading conditions. This was especially prevalent during the short circuit testing. A tachometer was used to capture the speed profile of any transients which was necessary to be incorporated into simulations later on. The switches shown in Figure 17 were used to insert loading conditions as well as short circuits in a controlled manner.

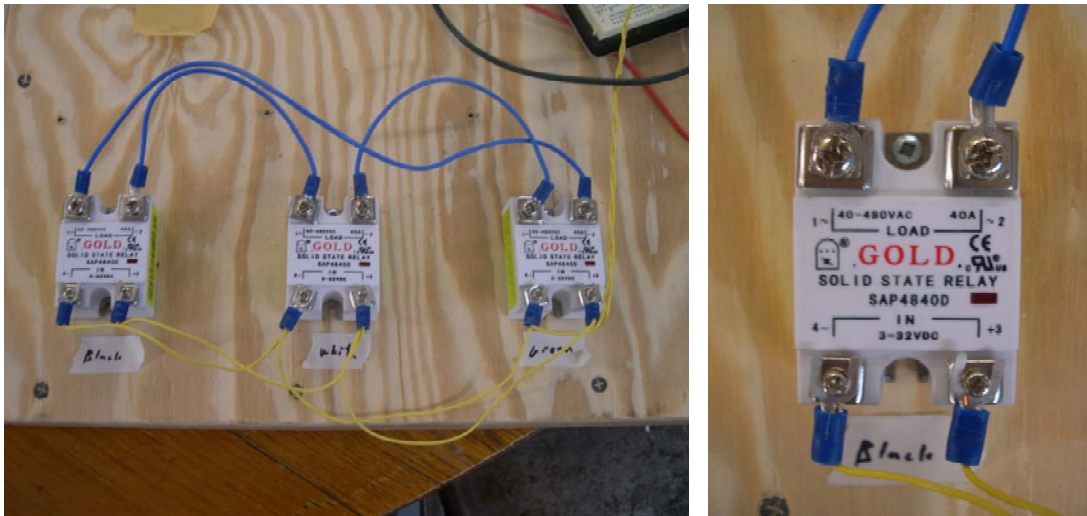


Figure 17: Switching Apparatus for short circuit implementation

TTL logic was used to have an adjustable trigger switch. A switch on duration of 52 ms was used when the generator was being short circuited. The generator was always open circuited in the initial condition and loads of progressively smaller resistances were applied to the generator. In much the same manner as we approached the fault condition the on times of the switch were raised until the generator reached 52 ms.

4.4.2 Test Results

Figure 18 below shows typical lab results obtained for the bench generator short circuit tests. These results show the tachometer results for the 1.5 HP motor. The tachometer is a Hall effect sensor that was placed in close proximity to the gears on the uncoupled side of the motor. The output of the tachometer was used to capture the speed profile of the generator during the short circuit transient.

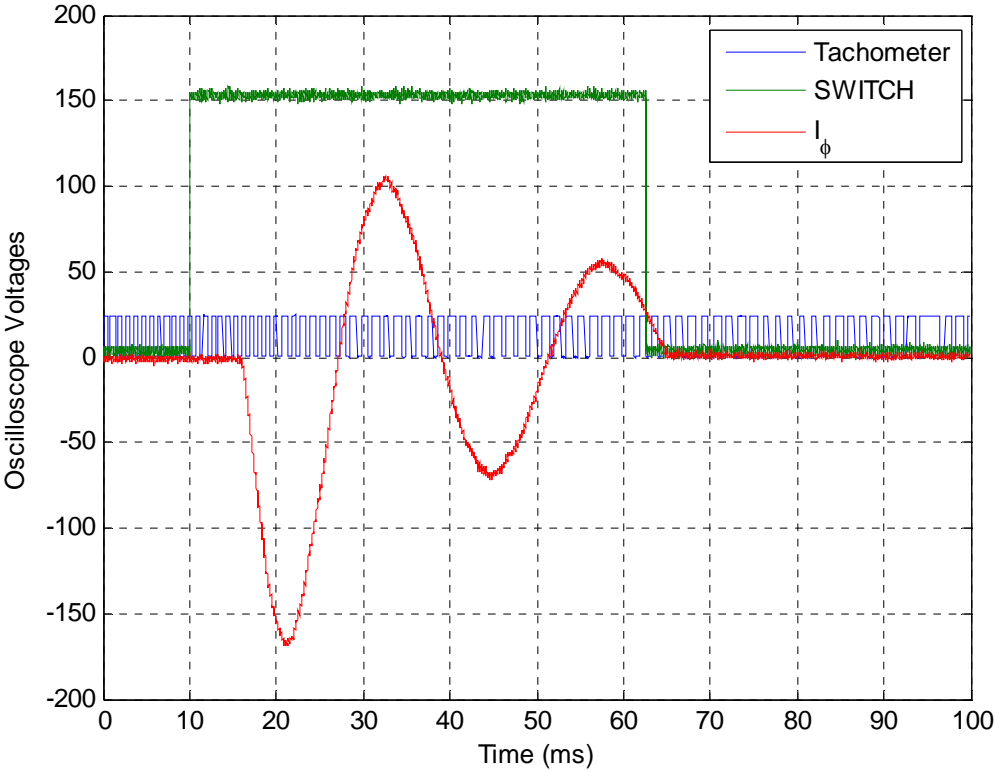


Figure 18: Short Circuit Results from Oscilloscope

The TTL voltage input to each of the three switches is also shown. In this example it was noted that there was a 6.6 ms delay from the time the voltage was applied to the switch until the switch was shut as indicated by the delay in short circuit line current. The same delay was apparent in the opening of the switch. The delays were consistent for each of the three switches and did not affect the short circuit results.

Figure 19 below shows the field current response during the short circuit. In the steady state prior to the short circuit the field current is constant (approximately two amps) and,

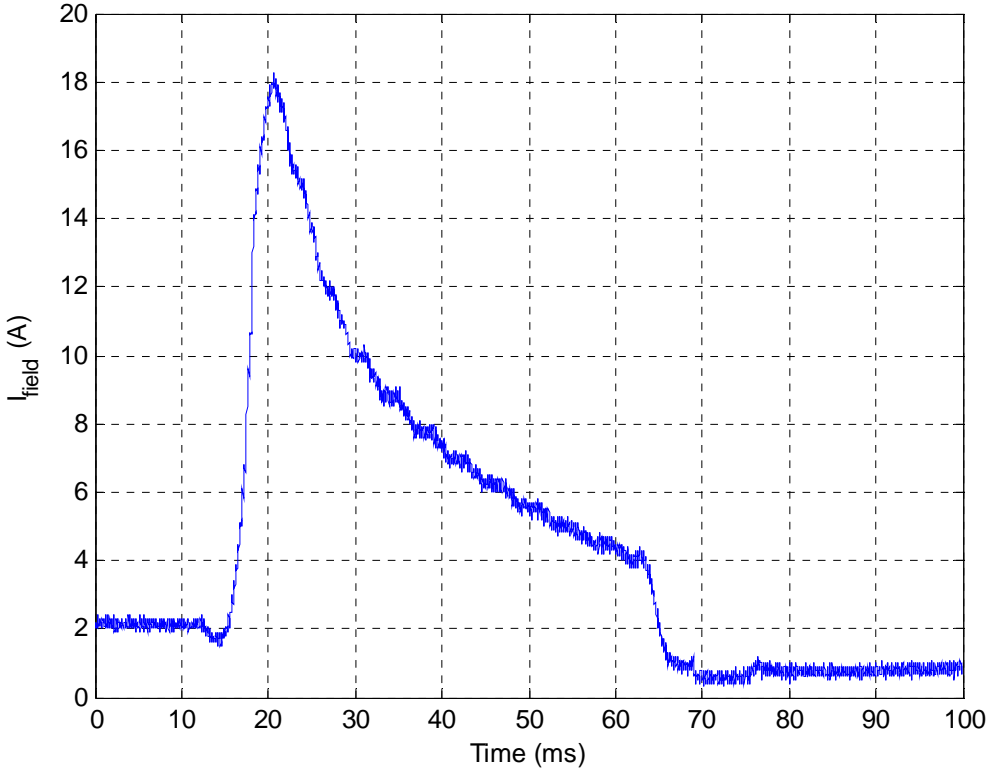


Figure 19: Field Current during short circuit

correspondingly, the flux linkages in the field winding are constant. At this point the stator currents are zero and therefore do not contribute to the field flux linkages. Once the stator currents start in the short circuit condition they lag the internal voltages by 90° which causes a demagnetizing armature reaction flux in the field winding. This armature reaction opposes the field flux. From the conservation of flux linkages, and assuming the field resistance equal to

zero we get the result that the field flux will remain constant. The field resistance is not zero, but is small in value, therefore for a small time interval such as seen above we can assume that the field flux will be approximately constant (8). As a result of the demagnetizing component of the stator currents the field current must increase. Figure 20 shows the speed profile of the bench generator. The first speed profile shown is as a result of the tachometer connected to the 1.5 HP DC motor. The second profile is as a result of the simulation which will be discussed in the next chapter. The results match each other with the exception of the choppiness of the tachometer waveform. For the simulation the speed profile, based on the inertia constant was used. The parameter necessary for converting the tachometer to frequency is the gear ratio of the generator to the motor which is (12/32). When the DC motor is operating at 4800 RPM the generator is turning at 1800 RPM which equates to an electrical frequency of 60 Hz.

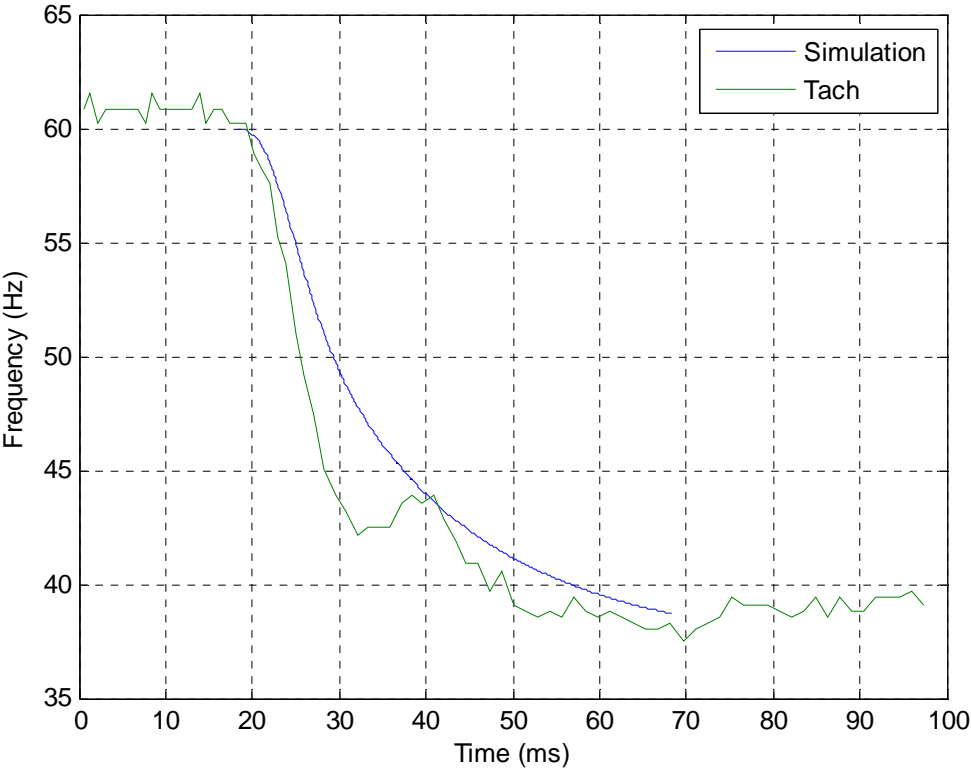


Figure 20: Speed profile for Short Circuit (Tachometer and Inertia Constant)

4.4.3 Analysis of Data

As stated previously, the purpose of the short circuit testing was to obtain the transient and sub-transient reactances (X'_d and X''_d) as well as the transient and sub-transient short circuit time constants (t'_d and t''_d) for the bench generator. Figure 21 shows how X'_d was evaluated.

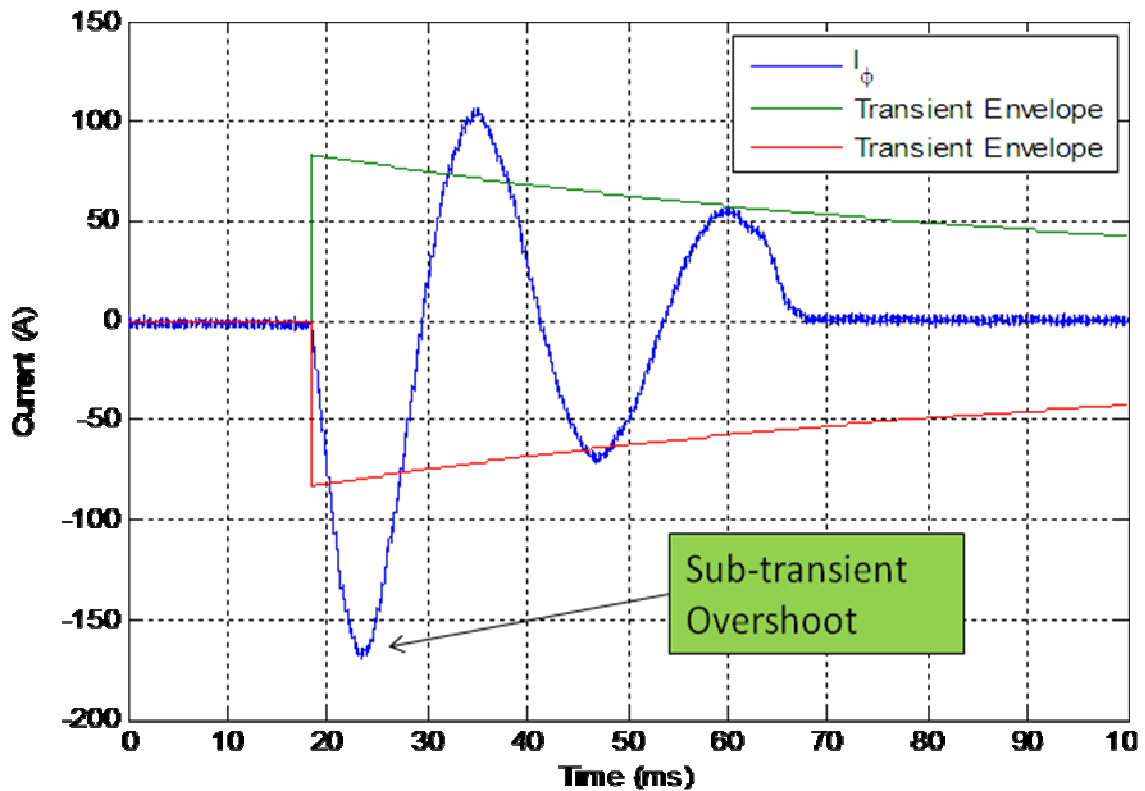


Figure 21: Evaluation of X'_d

There is a typical range of values (9) associated with direct axis transient reactances (0.17-0.37 per unit) which was the starting point for the determination of the short circuit time constants. The reactances must be matched to Figure 21 above, matching the classical short circuit equation, as well the bench generator “Equal Mutuals” model which will be discussed in the next chapter. The method employed was to assume that there was no sub-transient reaction and that the short circuit response was entirely as a result of transient reactance. The transient envelope using Equation 3 is shown in Figure 21 above. The short circuit current corresponding to 60 ms

was matched to the transient envelope as this was the last actual datum point available. It is then apparent that the initial assumption of no sub-transient component is not a valid one. There is a sub-transient component for the generator response since the short circuit current is not bound by the transient envelope. Therefore, what is shown above is the transient envelope that was matched to the “Equal Mutuals” model. This corresponded to a short circuit transient time constant of 45 ms and a transient reactance of 0.197 Ω per unit.

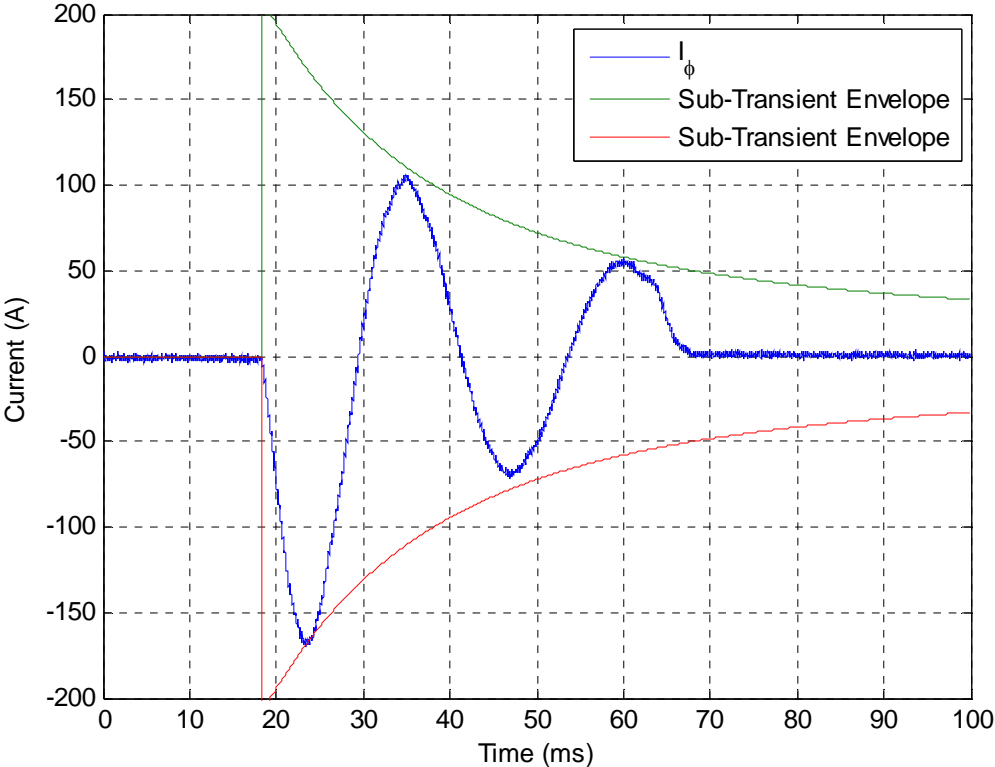


Figure 22: X_d'' Determination

It is now possible to obtain the sub-transient reactance and short circuit time constant. In a similar fashion to choosing the transient reactance, X_d'' was chosen to satisfy the “classical” short circuit equation as shown in Figure 22 above as well as producing a good result in the chapter five simulations. T_d'' can then be chosen to match the short circuit response to the sub-transient envelope shown above. There is not a perfect match of the sub-transient envelope to the short circuit current shown above. The solution of T_d'' equal to 15 ms and X_d'' equal to 0.094 Ω per

unit was chosen based on minimizing errors with both the classical equation as well as the simulation discussed in the next chapter.

Chapter 5

This chapter takes the laboratory results from chapter 4 and uses the equal mutual model to simulate the DDG and bench generators. The simulation models allow direct comparison of the two generators. This chapter will summarize those results and determine feasibility for hardware emulation.

5.0 Generator Modeling

Now that the physical parameters of the bench generator are known the next step is to use those parameters to simulate the generators short circuit response. Once the simulation matches the actual response for the bench generator it is then possible to use the DDG-51 plant parameters to simulate its short circuit response. At this point we can compare the differences between the two generator responses and present a conclusion on how the bench generator results can be used to assess how the DDG-51 plant would respond. Validation of the model used will be accomplished by looking at actual short circuit data (10). The simulation results are assumed validated when the simulation results match the known response.

5.1 Equal Mutuals Modeling

The list of parameters that were unknown prior to the short circuit analysis are shown below. These are the values that are necessary to be identified in order to accomplish a short circuit simulation of the synchronous generator.

1. Inertia Constant H – This constant relates the actual moment of inertia of the mechanical rotating components to a base of electrical volt amps. The speed profile slowdown is known for the generator as a result of the tachometer. The inertia constant is used to match the model speed change to that seen in the laboratory.

$$H \equiv \frac{\text{Rotational kinetic energy at rated speed}}{\text{Base Power}} = \frac{J\omega_0}{2pT_B}$$

2. Direct Axis Reactances (X'_d and X''_d) - These values have a direct effect on both the Equal Mutuals model and with the short circuit “classical equation” analysis in the previous chapter. These parameters are obtained by matching the simulation model and the classical equation. The short circuit time constants can then be determined from the classical equation with the assumption that the dominant reaction for the bench generator would be from the transient reaction. The remainder of the short circuit reaction would be attributed to the sub-transient reaction.
3. Short Circuit Direct Axis Time Constants (T'_d and T''_d) - These constants determine the amplitude of the short circuit current response in the generator. Based on the analysis in Chapter four we have an initial range of values. The short circuit time constants do not have a direct impact on the equal mutuals model although they can be used to assess initially what other parameters could be.
4. Open Circuit Direct Axis Time Constants (T'_{do} and T''_{do}) - When the armature is open circuited the field circuit is no longer affected by the armature. The change of field current is dependent only on the field winding self-inductance and resistance. Therefore, the open circuit armature voltage is proportional to field current and has the same time constant as the field circuit. These values are determined from the equal mutuals simulation.
5. Quadrature Axis Reactances (X_q and X''_q) - The definitions for the quadrature axis reactances are the same as for the direct axis reactances except that the rotor is positioned such that the quadrature is in line with the crest of the magneto motive force wave. For the simplified two pole case shown in Figure 23 below it is apparent that the inductance for the quadrature axis would be less than the direct axis inductance. This is not, necessarily, the case for the sub-transient reactances and in fact the q-axis sub-transient reactance ends up being greater than the d-axis sub-transient reactance for the bench generator.

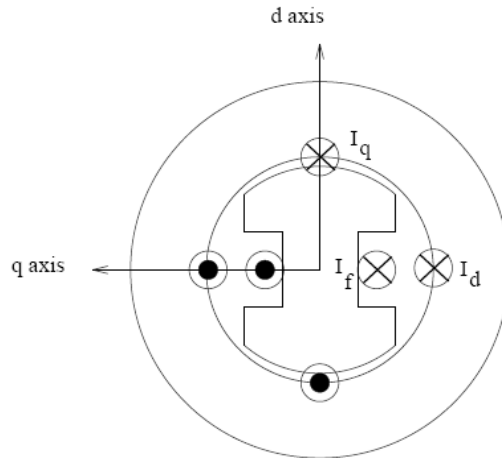


Figure 23: Direct and Quadrature Axes (6)

6. Open Circuit Quadrature Axis Sub-Transient Time Constant (T''_{qo}) – In a salient pole machine the transient time constant for the q-axis can be neglected (11) but T''_{qo} must be included in the model. Although the generator does not have explicit amortisseur windings there are current paths that produce the same effect. This parameter is determined in the model.

7. Armature Leakage Reactance (X_l) – This is the reactance which results from the difference between the total flux produced by the armature current acting alone and the space fundamental of the air gap flux. There are three components that make up X_l which are slot leakage, end winding, and differential leakage flux. This parameter is determined from the model.

5.1.1 Bench Generator Model

Referring to Figure 7 the equations for the direct axis reactance as well as the direct axis transient and sub-transient reactances can be written as shown below.

$$x_d = x_{al} + x_{ad}$$

The direct axis reactance is dependent on the magnetizing reactance as seen in Figure 7.

$$x'_d = x_{al} + x_{ad} \parallel x_{fl}$$

The transient reactance includes the effects of the field winding reactance.

$$x''_d = x_{al} + x_{ad} \parallel x_{fl} \parallel x_{kdl}$$

Finally, the sub-transient reactance is determined by also including the direct axis damping reactance. These are determined by circuit analysis of the circuit model shown in Figure 7.

These equations show that the transient reaction is defined by the field and magnetizing reactances in parallel whereas the sub-transient reaction includes the effects of the damping reactance. From these equations we can solve for the X_f and X_{kd} (see Appendix 3 and the MATLAB function MI.M for equations). The equations listed below can be used to solve for the field and damping resistances. However, it is important to note that these equations depend on the time constants being spread widely apart (6). It should also be noted that the bench generators field resistance was directly measured as opposed to using a calculated value.

$$T'_{do} = \frac{x_f}{\omega_o r_f}$$

Once again by looking at the circuit model shown in Figure 7 and knowing that the transient time constant is a function of the field winding and the sub-transient time constant includes the effects

of the damper winding it is determined that the sub-transient open circuit time constant is the following:

$$T''_{do} = \frac{x_{kdl} + x_{fl} || x_{ad}}{\omega_o r_f}$$

Initial estimates for T'_{do} and T''_{do} can be obtained by using the relationships shown below which are derived from Equation 5 with the assumption that T'_d is much greater than T''_d and that T'_{do} is much greater than T''_{do} . This turns out to be an adequate assumption to obtain an initial estimate for both T'_{do} and T''_{do} . (6)

$$T'_{do} = \left(\frac{x_d}{x'_d} \right) T'_d$$

$$T''_{do} = \left(\frac{x'_d}{x''_d} \right) T''_d$$

The equations showed to this point allowed for the calculation of the parameters that define the bench generator which are shown in Table 2. This was not finalized on the first iteration. This required several iterations which required looking at the simulated short circuit response and comparing it to the actual response as well as the calculated response using the classical short circuit equation. Once the simulated short circuit response matched the actual response those were the values that were assessed as correct and are as listed below.

P_{base} (Watts)	5000	x_{kdl}(Ω) p.u.	.0628
V_{base} (V)_{line-line} RMS	207.8	x_q(Ω) p.u.	.770
I_{base} (A)_{RMS}	13.9	x_d(Ω) p.u.	1.007
pf	0.8	x_{kq}(Ω) p.u.	.837
Pole Pairs	2	x_q^{''}(Ω) p.u.	.150
H (sec)	.190	x_d['](Ω) p.u.	.197
r_a (Ω) p.u.	.056	x_d^{''}(Ω) p.u.	.094
x_l (Ω) p.u.	.0500	x_f(Ω) p.u.	1.13
x_{aq} (Ω) p.u.	.720	x_{kd}(Ω) p.u.	1.020

$r_{kq} (\Omega) \text{ p.u.}$.0317	$t_{do}' (\text{sec})$.409
$x_{kql} (\Omega) \text{ p.u.}$.116	$t_{qo}'' (\text{sec})$.070
$x_{ad} (\Omega) \text{ p.u.}$.957	$t_{do}'' (\text{sec})$.030
$r_f (\Omega) \text{ p.u.}$.0126	$t_d' (\text{sec})$.045
$x_{fl} (\Omega) \text{ p.u.}$.173	$t_d'' (\text{sec})$.015
$r_{kd} (\Omega) \text{ p.u.}$.0185		

Table 2: Bench Generator Parameters

The values shown in yellow in Table 2 are the parameters that were adjusted in the simulation to match the simulated short circuit response to the actual short circuit response. These parameters had a direct effect on other calculated values shown in the table. The inertia constant was also changed but this was just to match the simulated frequency to the actual short circuit frequency. The inertia constant had no effect on the other calculated values in the table.

The model state equations shown below are derived with the assumption that the terminals are constrained by voltage (6). These are the equations used to model the bench generator and DDG-51 plants.

$$\frac{d\psi_d}{dt} = \omega_0 v_d + \omega \psi_q - \omega_0 r_a i_d$$

This shows that the time rate of change of direct axis flux is dependent on direct axis voltage. The base frequency (ω_0) for this machine is 377 rad/sec and does not change in the simulation model. However, the electrical frequency of the machine (ω) will slow down during the short circuit scenario. The direct axis voltage when the generator is short circuited is zero which simplifies the differential equation.

$$\frac{d\psi_q}{dt} = \omega_0 v_q - \omega \psi_d - \omega_0 r_a i_q$$

The time rate of change of quadrature axis flux is comparable to the direct axis flux with quadrature and direct subscripts switched. Similarly, in a short circuit scenario the quadrature voltage is zero.

$$\frac{d\psi_{kd}}{dt} = -\omega_0 r_{kd} i_{kd}$$

$$\frac{d\psi_{kq}}{dt} = -\omega_0 r_{kq} i_{kq}$$

The time rate of change of direct and quadrature damping fluxes are dependent simply on their respective resistances and transient currents. The resistances are the same as those shown in the circuit models (Figure 7 and Figure 8).

$$\frac{d\psi_f}{dt} = \omega_0 v_f - \omega_0 r_f i_f$$

The time rate of change of the field flux depends on the field voltage and field current. In the model used the field voltage was set to a constant voltage (32 volts) prior to the short circuit test. This field voltage when the armature is open circuited corresponded to rated armature voltage of 208 volts RMS phase to phase. The applied field voltage remains constant during the transient. The actual field current during the transient fault was inserted into the simulation as shown in the MATLAB function SF2.M in Appendix 3.

$$\frac{d\omega}{dt} = \frac{\omega_0}{2H} (T_e + T_m)$$

$$T_e = \psi_d i_q - \psi_q i_d$$

Equation 4: State Equations for Equal Mutuals Model

The slowdown of the bench generator was captured by using a tachometer. The tachometer results were then used to identify the inertia constant for the bench generator (H) shown in the

equation above. Since the generator was initially open circuited the mechanical torque T_m is zero. The inertia constant was changed until the simulation speed profile matched the tachometer speed profile. The simulation results were used instead of the tachometer speed profile since they matched.

It should be noted that for short circuit conditions the direct and quadrature voltages (v_d and v_q) are zero which will simplify the equations above. The armature resistance (r_a), field resistance (r_f), field current (i_f), and speed profile (ω) were all directly measured in the laboratory for the bench generator. All were directly input into the model with the exception of the speed profile. The speed profile was matched with the inertia constant, as discussed previously, and then entered into the model. This was accomplished to determine the inertia constant for the generator. For the short circuit scenario the torque angle (δ) is initially zero when open circuited and remains zero during the short circuit transient. As a result this equation is not used in the short circuit analysis. It is shown because it was used in the validation of the model as shown in Appendix 6.

The MATLAB simulation model (Appendix 3) results are shown in Figure 24 below for three phase short circuit currents. The simulation model (Appendix 3) has three functions that are called which are MI.M, MIQ.M, and SF2.M. The function MI.M calculates the direct axis parameters while MIQ.M calculates the quadrature axis parameters. The quadrature axis parameters are calculated in the same way as the direct axis parameters according to the circuit model shown in Figure 8. SF2.M is a function that uses the differential equations (Equation 4) discussed previously to determine the state variables. Appendix 5 is a users manual and explains in more detail how to use the simulation.

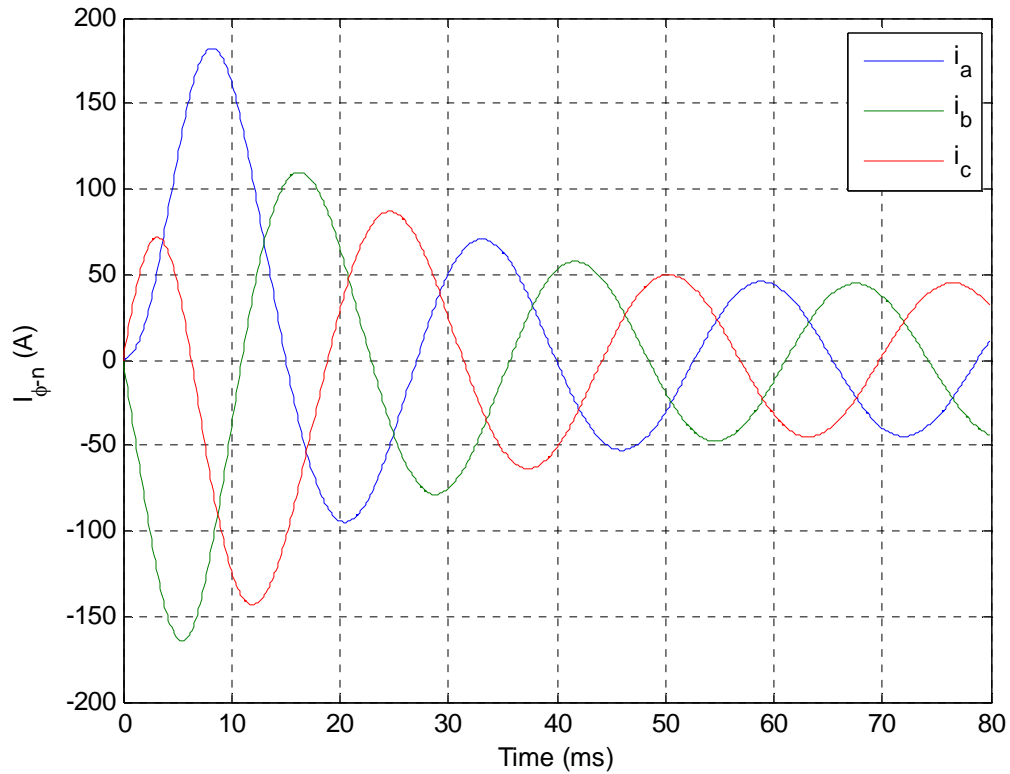


Figure 24: Bench Generator Simulation

The comparison of the simulation to the actual lab results are shown in Figure 25 as well as Table 3 below. Also shown for comparison are the short circuit currents as calculated with the classical equation. The results match within 0.1% for the first simulated peak compared to the actual data. The second short circuit peak has the highest error and then decreases to -0.7% at 42 ms. The most critical bench generator parameter to match is the first short circuit peak amplitude as ultimately the interest is in evaluating short circuit protective actions.

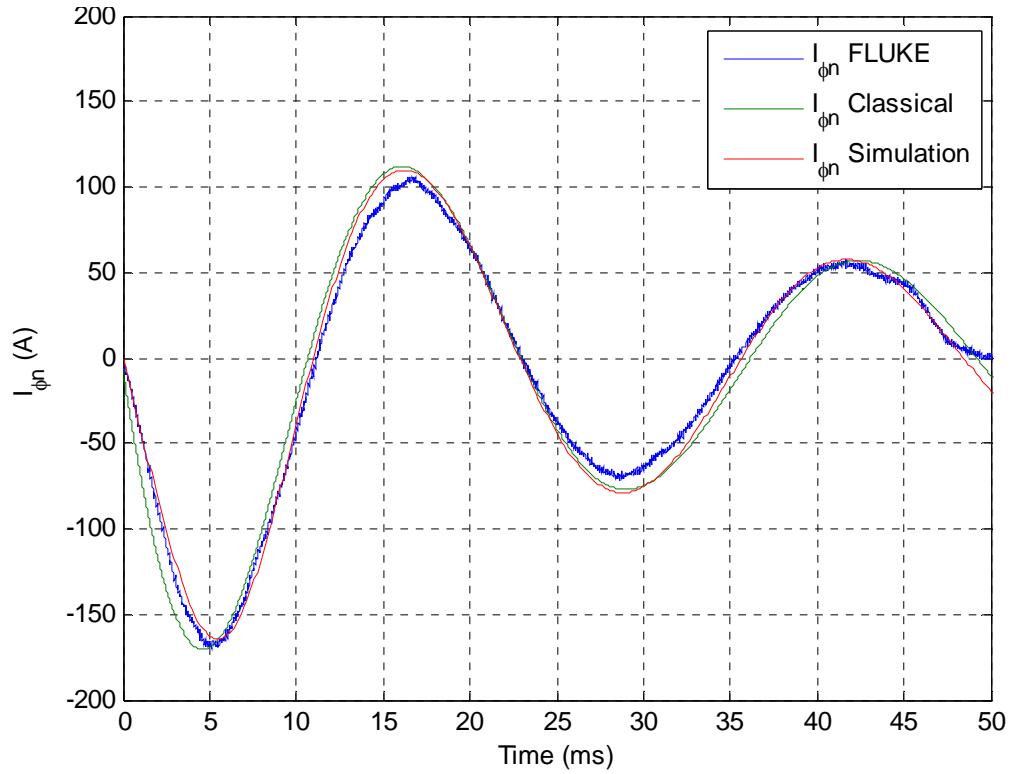


Figure 25: Bench Generator (Simulation, Classical, and Actual) Results

I_{phase}	Peak at 5 ms		Peak at 17 ms		Peak at 29 ms		Peak at 42 ms	
Actual (A)	170		106		72		58	
Classical (A)	170.6	0.4%	112.0	5.7%	76.9	6.8%	57.0	-1.7%
Simulation (A)	169.8	-0.1%	109.9	3.7%	77.4	7.5%	57.6	-0.7%

Table 3: Simulation and Classical results compared to Actual Data

5.1.2 Sensitivity Analysis

A sensitivity analysis was conducted on the yellow parameters listed in Table 2 to understand which parameters are having the biggest impact on the equal mutuals model. The results are shown below in Table 4.

Sensitivity Parameter	Actual Value	Short Circuit Peak Percent Decrease (%) due to 10% decrease in sensitivity parameter	Short Circuit Peak Percent Increase (%) due to 10% increase in sensitivity parameter
x_q (p.u.)	0.77	0.03	0.05
x_q'' (p.u.)	0.15	1.3	1.3
x_d' (p.u.)	0.197	-0.5	-0.6
x_d'' (p.u.)	0.094	-6.5	-5.9
t''_{qo} (sec)	0.07	-0.05	-0.03
t''_{do} (sec)	0.03	0.7	0.6

Table 4: Bench Generator Model Sensitivity Parameters (First Peak Current)

The most difficult item to match in the equal mutuals model was the first short circuit current peak at 6 ms corresponding to phase b current as shown in Figure 25. This was a peak value of 170 amps in the actual short circuit test. This peak value for phase current was used to assess the sensitivity numbers shown in the table. A sensitivity parameter was changed either plus or minus ten percent and the peak current percent change was assessed. A negative percentage change corresponds to peak current increasing for a decrease in a sensitivity parameter or vice versa. The most sensitive parameters were the sub-transient d-axis and q-axis reactances respectively (highlighted in yellow in the table). This result is anticipated based on the parameter chosen to be assessed which is predominately a sub-transient item (i.e. the first peak current).

Another sensitivity analysis was conducted on the decay amplitude at 42 ms. This was looked at to determine the sensitivity of the decay envelope of the short circuit current as a result of changing the same parameters listed in Table 2. The first peak amplitude and the last peak amplitude for the short circuit currents were mutually dependent on the sensitivity parameters identified.

Sensitivity Parameter	Actual Value	Short Circuit Envelope Percent Decrease due to 10% decrease in sensitivity parameter	Short Circuit Envelope Percent Increase due to 10% increase in sensitivity parameter
x_q (p.u.)	0.705	-0.2	-0.5
x_q'' (p.u.)	0.243	-0.4	-0.1
x_d' (p.u.)	0.197	-7.4	-6.7
x_d'' (p.u.)	0.0579	3.7	2.9
t''_{qo} (sec)	0.0672	0.9	0.7
t''_{do} (sec)	0.048	3.4	3.5

Table 5: Bench Generator Sensitivity Parameters (Decay Envelope)

The sub-transient q-axis open circuit time constant and q-axis reactance had little effect on either the first peak amplitude for short circuit current or the decay envelope as shown in Table 5. The most sensitive parameter for affecting both the first peak amplitude and the decay envelope in the simulation was the sub-transient d-axis reactance and therefore care must be taken when adjusting this parameter.

5.1.2 DDG Model

The equal mutuals model developed for the bench generator was used to simulate a three phase short circuit for a DDG electrical generator. The model used plant parameters for two DDG plants as provided in Table 6 below to run two different simulations.

	DDG-I	DDG-II		DDG-I	DDG-II
P_{base} (KVAR)	3125	3125	x_{kdl}(Ω) p.u.	0.333829	0.400595
V_{base} (V)_{line-line RMS}	450	450	x_q(Ω) p.u.	1.08	1.296
I_{base} (A)_{RMS}	4009	4009	x_d(Ω) p.u.	1.848	2.2176
pf	0.8	0.8	x_{kq}(Ω) p.u.	1.3298	1.5957
Pole Pairs	2	2	x_q'(Ω) p.u.	0.328	0.3936
H (sec)	2.137	1.7083	x_d'(Ω) p.u.	0.207	0.2484
r_a (Ω) p.u.	0.00515	0.00618	x_d''(Ω) p.u.	0.172	0.2064
x_l (Ω) p.u.	0.08	0.096	x_f(Ω) p.u.	1.9048	2.2858
x_{aq} (Ω) p.u.	1	1.2	x_{kd}(Ω) p.u.	2.1018	2.5222
r_{kq} (Ω) p.u.	0.0613	0.07356	t_{do}'(sec)	4.7846	4.7846
x_{kql} (Ω) p.u.	0.329787	0.395744	t_{qo}''(sec)	0.10081	0.10081
x_{ad} (Ω) p.u.	1.768	2.1216	t_{do}''(sec)	0.048521	0.048521
r_f (Ω) p.u.	0.00111	0.001332	t_d'(sec)	0.5553	0.5553
x_n(Ω) p.u.	0.136829	0.164195	t_d''(sec)	0.038912	0.038911
r_{kd}(Ω) p.u.	0.023968	0.028762			

Table 6: DDG-51 generator parameters provided by NAVSEA

The values indicated in the un-shaded blocks above were provided by NAVSEA and the shaded parameters were calculated from the provided values (Appendix 7). The equal mutuals model allows for the generator to be at different loading levels prior to the short circuit. Two separate simulations were run with the DDG-I parameters, the first scenario of which was for the generator unloaded and the second scenario was for the generator fully loaded at rated capacity. These results are shown in Figure 26 and Figure 27. The results for the DDG-II parameters were similar to the DDG-I results and are shown in Appendix 4.

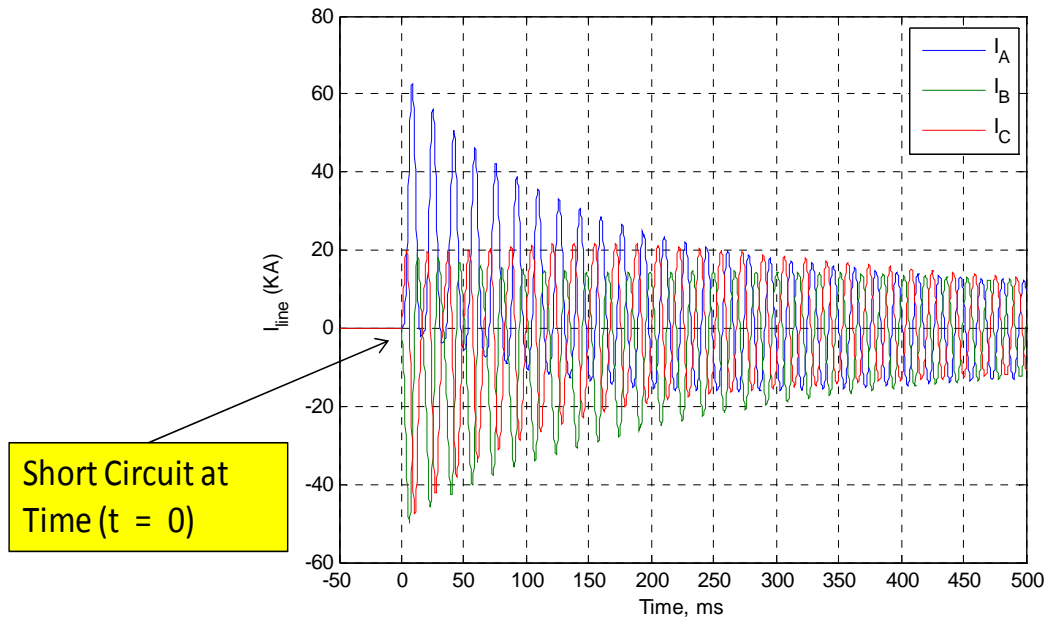


Figure 26: DDG-I Short Circuit (Initially Unloaded)

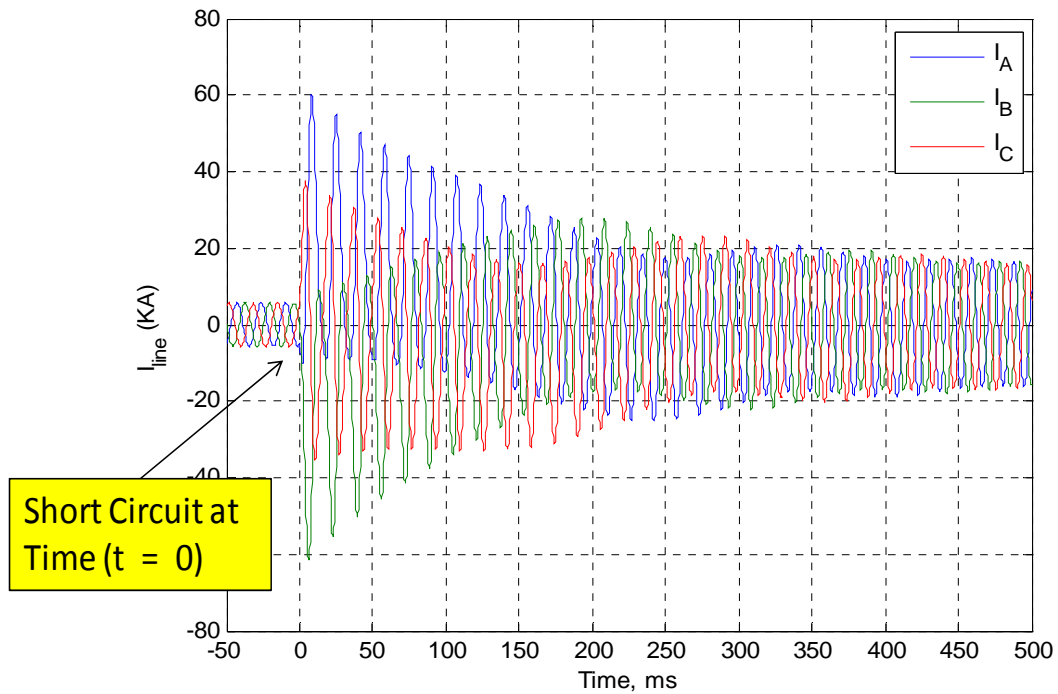


Figure 27: DDG-I Short Circuit (Initially Fully Loaded)

5.2 DDG and Bench Generator Comparison

Referring to Figure 7 we can observe that the terminal impedance will have a second order numerator and a second order denominator. The terminal impedance can be written in terms of the transient reactance (x_d), transient short circuit and open circuit time constants (T'_d and T'_{do}), as well as the sub-transient short circuit and open circuit time constants (T''_d and T''_{do}). (6)

$$x(s) = x_d \frac{(1 + T'_d s)(1 + T''_d s)}{(1 + T'_{do} s)(1 + T''_{do} s)}$$

Equation 5: Per Unit Inductance, Synchronous Generator

From section 4.1 it was observed that the bench generator has a more rapid response than the DDG-51 generator. The bench generator transient response is 11.68-12.44 times faster than the DDG response and the sub-transient response is 1.6 – 2.6 times faster. This is shown in the pole zero plot in Figure 28.

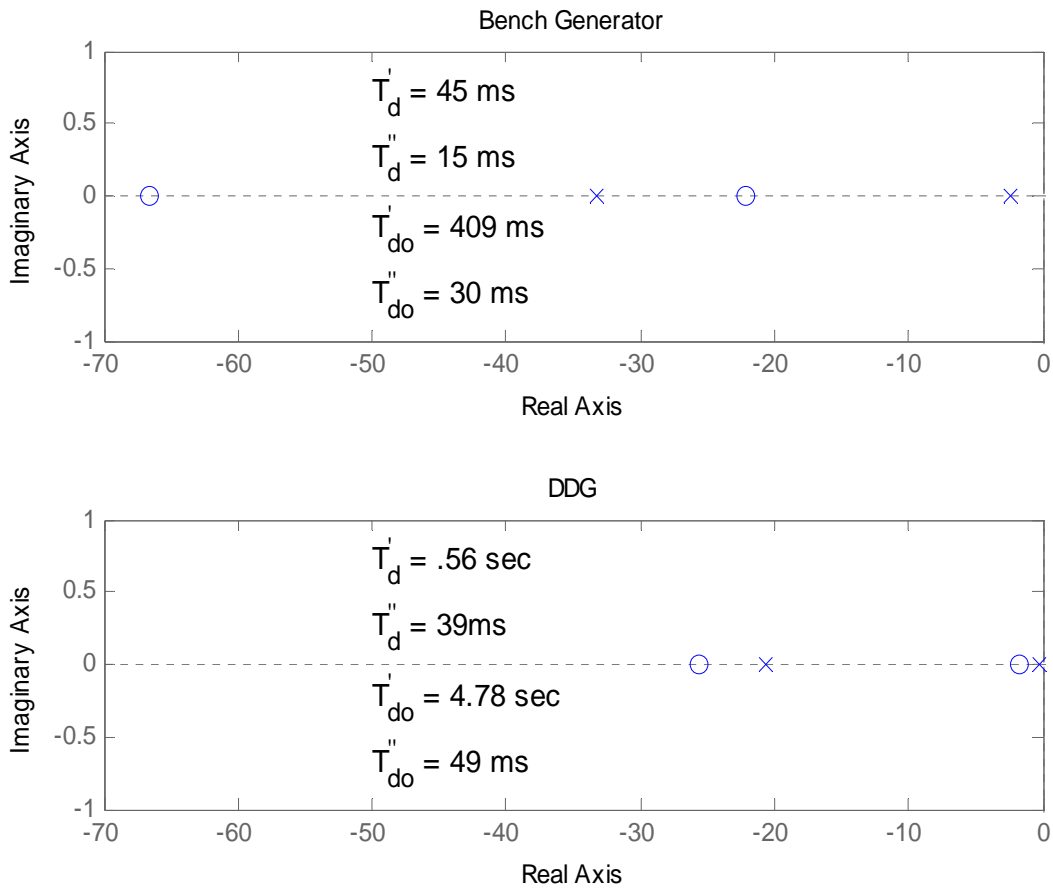


Figure 28: Pole Zero Plots for Bench Generator and DDG-I Model

From these results and the impedance magnitude plots in Figure 29 it is possible to compare the bench generator and DDG generator responses with each other.

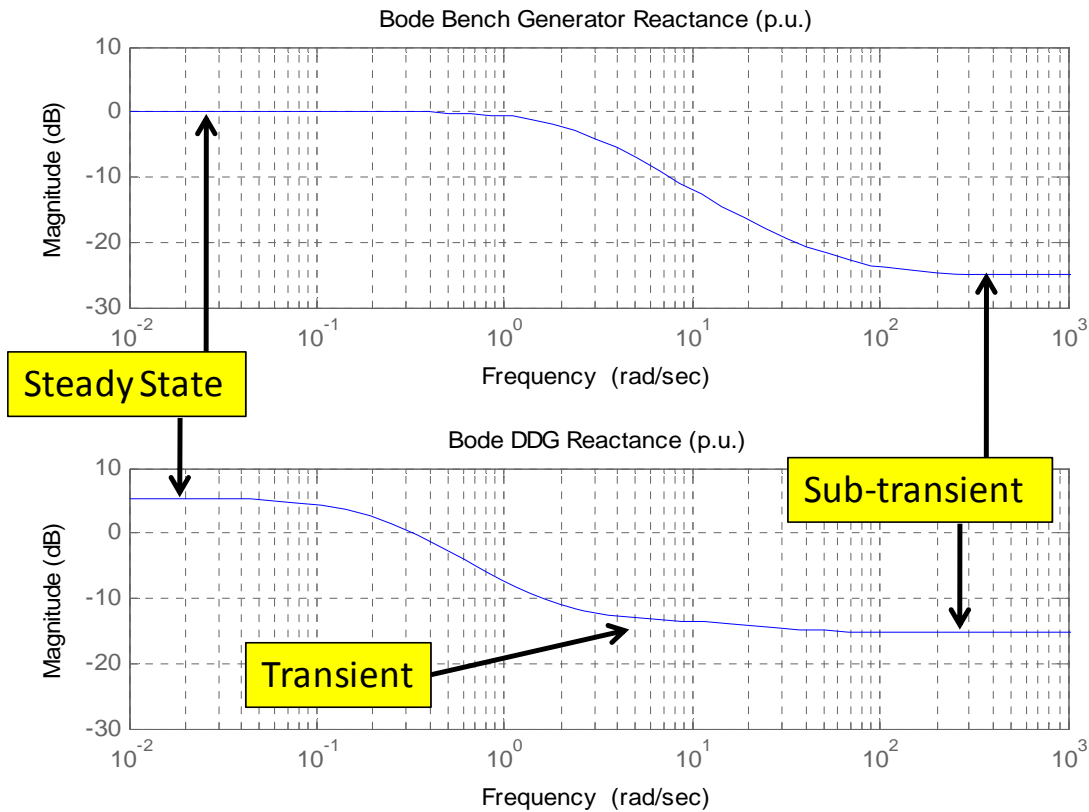


Figure 29: Impedance Bode Plots (Bench Generator and DDG-I)

It is apparent from the Bode plots that the DDG generator has three defined regions that are visible in Figure 29. For the DDG generator up to approximately $0.2 \frac{rad}{sec}$ is the steady state region, from approximately $(3 - 10) \frac{rad}{sec}$ is the transient region, and greater than approximately $60 \frac{rad}{sec}$ is the sub-transient regime. The bench generator has well defined steady state and sub-transient regions but there is not a well defined plateau for the transient regime. This is not a problem for the modeling being accomplished and may not, in fact, be a problem at all. If the magnitude response is determined more accurately in future studies by conducting a frequency response at the stator terminals it would be possible to match the Bode response more accurately in the future by adding additional poles and zeros to Equation 5. For the purposes of the modeling being conducted the concern is not to match the transient Bode magnitude response but

instead to capture the sub-transient response. This allows us to look at fault detection times and compare those to fault detection times for the DDG-51.

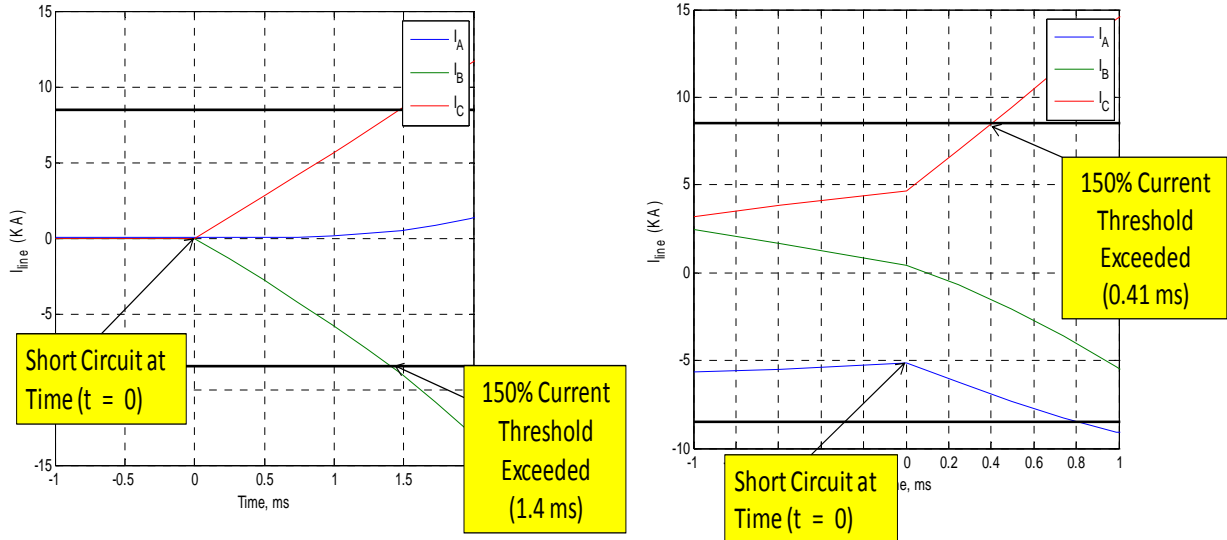


Figure 30: DDG-51 Current Threshold after Three Phase Fault (Initially Unloaded – Left), (Initially Fully Loaded - Right)

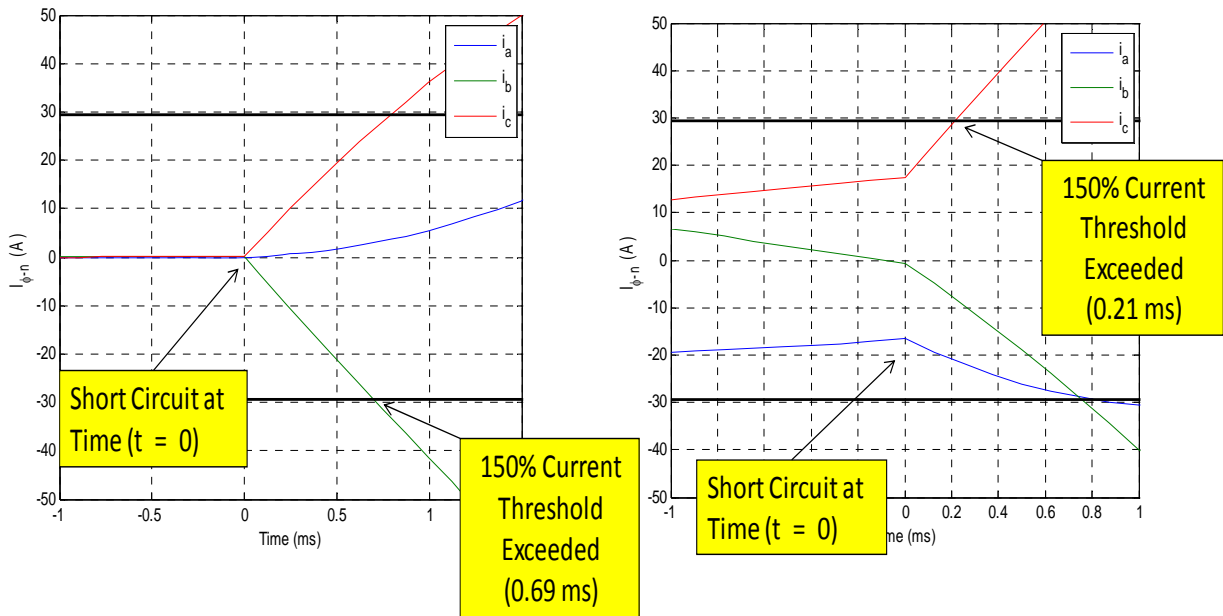


Figure 31: Bench Generator Current Threshold (Initially Unloaded – Left), (Initially Fully Loaded - Right)

Figure 30 and Figure 31 show the length of time for a three phase fault to cross a current threshold of 150% of rated capacity for both the bench and DDG generators (indicated at 29.46 and 8504 amps respectively). Both of these generators are shown with initial conditions of open circuited terminals (i.e. unloaded) as well as the case of a generator that is fully loaded. This 150% rated current threshold was used as a reference point to compare the DDG and bench generator responses to the approximate amount of time that would be necessary for the High Speed Relay (HSR) algorithm to detect a fault and determine whether or not the fault was downstream or not. This was used in lieu of a power calculation since the phase to phase terminal voltages in the modeling employed was zero volts. The 150% current threshold is a conservative estimate when compared to the power threshold used in the HSR algorithm and is a good datum point to start assessing fault detection capabilities for NILM testing. The figures above show all three phases of current simultaneously during the fault scenarios. The times listed for the fault threshold crossing correspond to the first phase of current which crosses this threshold. The bench generator and DDG currents were at the same exact phases at the time of the simulated three phase fault and therefore can be related to each other. Two observations are that number one the threshold is crossed faster when either the bench or DDG generator is fully loaded and number two that the threshold is crossed faster for the bench generator compared to the DDG generator in both situations. Figure 32 below shows actual fault data corresponding to the bench generator. The equal mutuals model predicts a current threshold crossing for the bench generator, when initially unloaded, of 0.69 milliseconds whereas the actual data shows a threshold crossing at 0.90 milliseconds. This difference is dependent on the particular phase of current that is captured. Note that the simulation shows each phase of current exceeding the 150% limit over a time range.

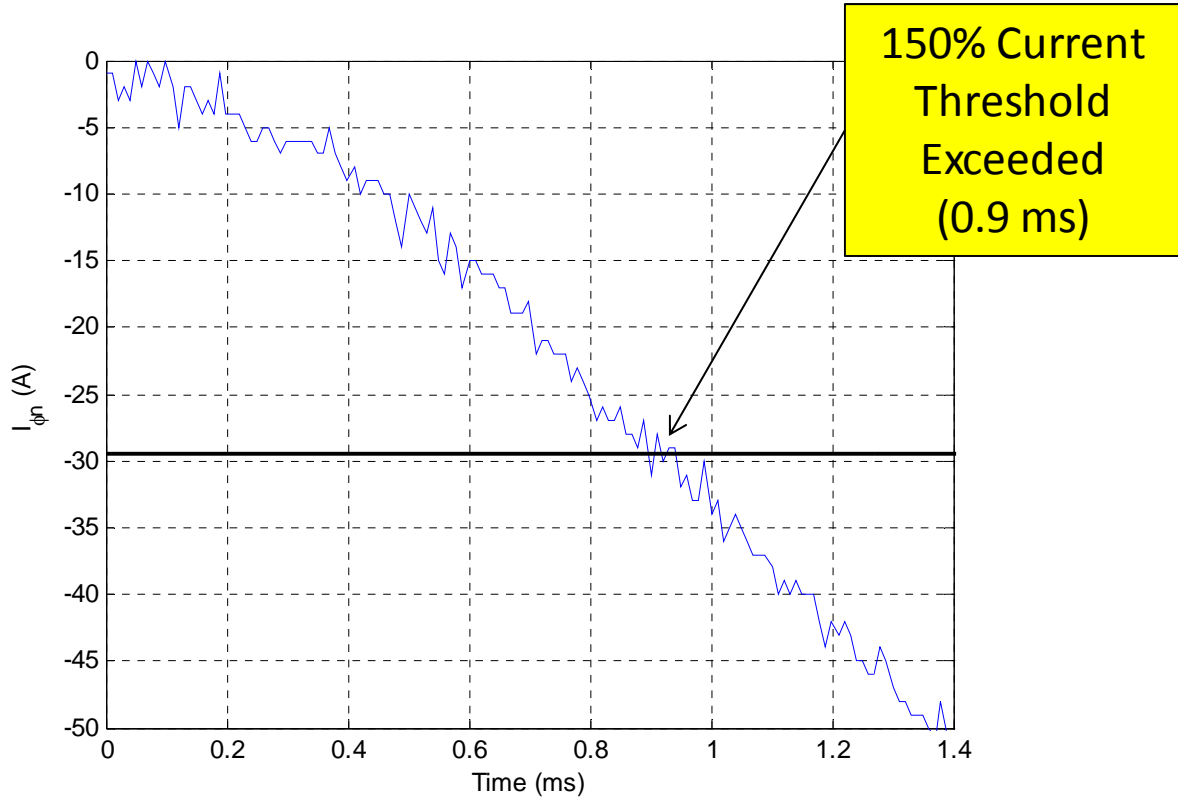


Figure 32: Bench Generator Actual Phase Current Crossing 150% Threshold

Table 7 below summarizes the times to exceeding the current threshold as well as indicating the initial rate of current increase. For the bench generator the actual as well as the simulated time is shown for the unloaded condition since that data point was available. For the rest of the scenarios just the simulated time is shown.

	Time (ms)	Current Rate (A/ms)
Bench Generator (Initially Unloaded)	0.90 (Actual)	32.7 (Actual)
	0.69 (Simulated)	42.7 (Simulated)
Bench Generator (Initially Fully Loaded)	0.21	140.3
DDG (Initially Unloaded)	1.4	6075
DDG (Initially Fully Loaded)	0.41	20742

Table 7: Generator Times for Fault Detection (150% Current)

5.2.1 Armature Reaction for DDG and Bench Generator

The armature reaction is clearly visible for the case of the DDG simulation but decays rapidly for the case of the bench generator as seen in Figure 24 thru Figure 27. The equation for the armature time constant, which determines how rapidly the DC offset decays to zero, is shown below.

$$T_a = \frac{x_2}{\omega r_a}$$

The negative sequence reactance (x_2) is equal to $\sqrt{X_d'' * X_q''}$. The armature time constants for the DDG and bench generator are shown in Table 8 below.

	r_a (Ω) p.u.	x_d'' (Ω) p.u.	X_q'' (Ω) p.u.	x_2 (Ω) p.u.	T_a (ms)
Bench Generator	.056	.094	.150	.119	5.6
DDG	.00515	.172	.328	.238	122.0

Table 8: Armature time constants for DDG and Bench Generator

To illustrate the effects of the armature reaction on the short circuit currents the simulation in Appendix 4 was run on the DDG parameters for three cases. The first case used the actual DDG parameters while the second and third case used armature resistances of ten times and twenty times the actual DDG armature resistance listed in Table 8. This had the effect of reducing the armature time constant to 12.2 and 6.1 milliseconds respectively. The results are shown in Figure 33 and show that the armature reaction is another important difference between the DDG and bench generators. Whereas the bench generator short circuits are primarily a result of the sub-transient and transient reactances and time constants the DDG generator also has a significant armature component.

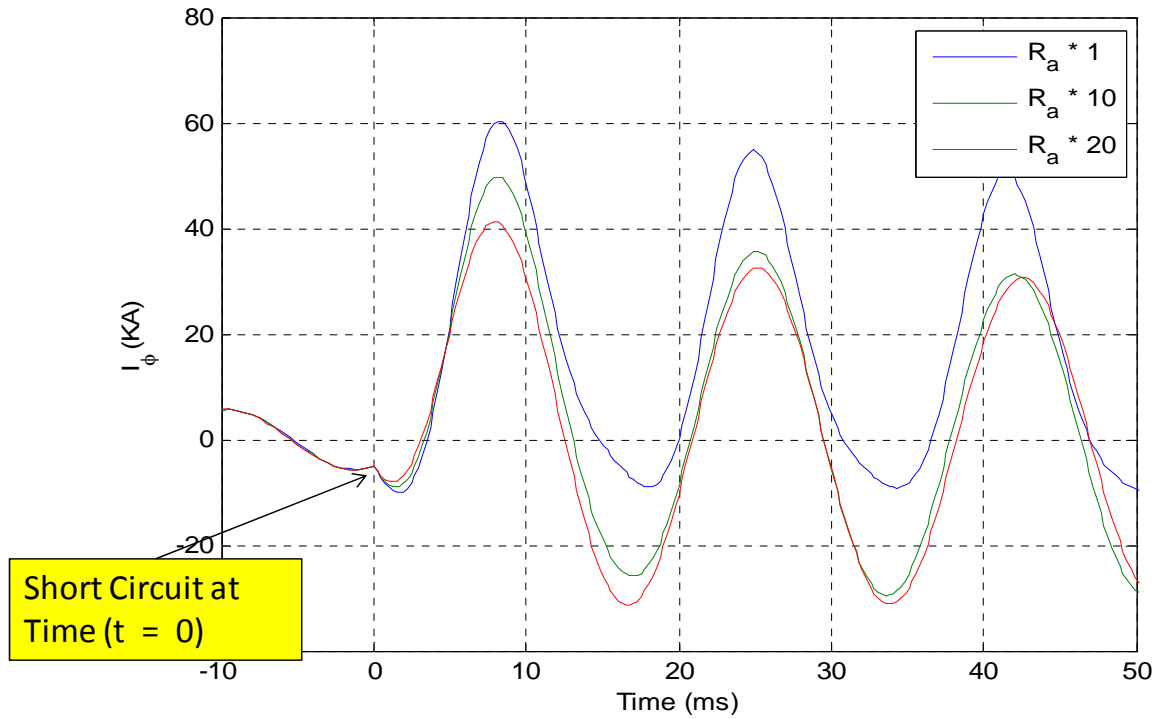


Figure 33: Effect of Armature Resistance on Short Circuit Current for DDG

In summary, the bench generator has a quicker response time than the DDG generator. In fact, for the loaded condition the bench generator is 1.78 times faster than the DDG whereas for the unloaded case the bench generator is 1.53 times faster. This means that when fault detection and protective action testing starts to be evaluated for the bench generator it can be compared to the DDG generator. If a fault detection and protective action can be shown to be effective for the bench generator than a case could be made that the protective action would be effective for the DDG plant which has a slower response time.

Chapter 6

6.0 Future Studies

The bench generator actual lab results have been compared to the equal mutuals model simulation results and match within 1.1% for the three phase short circuit time for current to cross the 150% threshold set point, as well as matching initial peak current amplitude within 0.1%. Further testing and validation of simulation and lab results are required to validate the bench generator model but the results so far are encouraging. Enough validation has occurred to this point start to start building and testing the bench generator electrical distribution system. The electrical distribution system will consist of three bench generators that will supply separate electrical distribution panels that are separated by circuit breakers. The setup will be consistent with a typical DDG electric plant configuration.

6.1 Additional Work

The equal mutuals model that was employed consisted of one set of damper windings for the direct and quadrature axes. It was shown in chapter four that the direct axis terminal did not have a well defined transient impedance for the bench generator (Figure 29). This was a result of the transient short circuit time constant being relatively close to the sub-transient open circuit time constant. It is possible to apply a low voltage across the stator terminals and vary the frequency from 10^{-3} – 100 Hz to determine the frequency response of the synchronous generator. This can be done with the rotor aligned to both the direct and quadrature axes to obtain information about both $X_q(s)$ and $X_d(s)$ (10). Once the frequency information is obtained it would then be possible to match the frequency response more accurately by using as many damper windings as required as opposed to the single winding that was used in the analysis presented thus far. This could then be used to validate the results presented in this thesis. It is important to note that the bench generator simulation based on one set of direct and quadrature windings is producing simulation results that match the sub-transient response. The transient response (i.e. between sub-transient and steady state) in the equal mutuals simulation may be

able to be matched further pending the results from the frequency response testing. If, however, the results of the frequency response testing match the Figure 29Bode results for the bench generator than the one damper winding model is sufficient for the simulation.

The next important step is to use the electric modeling results from this thesis and the speed modeling results (12) to build the mock DDG electric plant. From this it will be possible to simulate typical loads on an electrical distribution system and to start collecting NILM data to be used for fault detection analysis. Finally, a system of circuit breakers set up to simulate a DDG electric plant could be controlled by outputs from NILM based on the data collected from the NILM current and voltage sensors. The NILM outputs would be programmed to trip the circuit breakers to protect the electrical distribution panels based on manually inserted faults. Data collected would be used to determine optimal power thresholds to determine if the fault is downstream or upstream.

6.2 Conclusion

The synchronous generator modeling accomplished has been for the purpose of demonstrating that testing results from the bench generator can be related to a DDG plant. It has been shown that the bench generator has a faster electrical response than the DDG plant using the results from the equal mutuals model simulations. It is not a disadvantage that the bench generator has faster electrical characteristics than the DDG plant since if NILM can be shown to provide a benefit for fault detection and protection on the bench generator platform it stands to reason that it would provide the same benefit to the slower responding DDG plant. A main benefit of the NILM would be in assisting the MFM with HSR algorithm. As stated previously it is a lemma of this thesis that NILM could be used to provide real time fault threshold tuning for a DDG plant. Chapter five results have shown that the amount of time to cross the 150% rated current capacity, as well as the highest current peak amplitude, depends on the initial loading of the generators. Currently, MFM with HSR algorithm have a fault detection threshold that is adjusted to prevent false detections. This threshold is currently set independently of generator loading, and in fact must be set for the worst case loading condition which would be when the generators are lightly loaded. Switching transients, which occur in any electrical distribution system, are the main reason why fault thresholds need to be set higher. NILM could be used to identify

these switching transients and have a logic system that prevents them from being classified as faults. This would allow for the further optimization of fault set points by not having to set the threshold above these switching transient amplitudes. The next stage of NILM feasibility for fault detection and switchboard protection is ready to commence based on the results of the generator testing and simulations discussed in this thesis. This will be accomplished by testing on a mock DDG electric plant using three synchronous bench generators.

BIBLIOGRAPHY

1. **NAVSEA.** *A Guide to MFM III Operation.* Philadelphia : NSWCCD-SSES.
2. **Wipf, David P. and Parker, B.Eugene.** *Demonstration and Assessment of High-Speed Relay Algorithm.* Bethesda : Naval Surface Warfare Center, 1997.
3. **Proper, Ethan.** *Automated Classification of Power Signals.* Cambridge : Massachusetts Institute of Technology, 2008.
4. *Next Generation Integrated Power System.* s.l. : NAVSEA, 2007.
5. **Fitzgerald, A. E., Kingsley, Charles and Umans, Stephen D.** *Electric Machinery.* New York : McGraw-Hill, 2003.
6. **Kirtley, James L.** 6.685 Electric Machines. *MIT Open Courseware.* [Online] 2005. <http://ocw.mit.edu/OcwWeb/Electrical-Engineering-and-Computer-Science/6-685Fall-2005/CourseHome/index.htm>.
7. **Gross, Charles A.** *Electric Machines.* Boca Raton : CRC Press, 2007.
8. **Bergen, Arthur R.** *Power Systems Analysis.* Englewood Cliffs : Prentice Hall, 1986.
9. **Sheldrake, Alan L.** *Handbook of Electrical Engineering.* West Sussex : John Wiley & Sons Ltd, 2003.
10. **Krause, Paul C., Wasynczuk, Oleg and Sudhoff, Scott D.** *Analysis of Electric Machinery.* New York : Institute of Electrical and Electronics Engineers, Inc., 1995.
11. **Kimbark, Edward Wilson.** *Power System Stability.* Piscataway : IEEE PRESS Marketing, 1956.
12. **Elkins, Gregory.** *Hardware Model of a Shipboard Generator.* Cambridge : Massachusetts Institute of Technology, 2009.
13. **Leeb, Steven B. and Cox, Robert.** *Whitepaper: Role of the Combat Power Monitor in Zonal Electrical Distribution in the NGIPS.*

APPENDIX 1 - MATLAB Evaluation of Xd

```
% OCC and SCC Curves from Raw Lab Data called with OCCandSCC.m
% Gross page 264 [7] Electric Machines
% This matlab code does not call any other functions and is self sufficient

clear all;

% Lab Data

% OCCIf and OCCEa are laboratory obtained values

OCCIf = [0 0.09 0.12 0.19 0.27 0.31 0.41 0.44 0.52 0.57 0.63 0.74 0.76 0.81 0.91 0.96 1 1.09
1.14 1.24 ...
1.24 1.32 1.39 1.46 1.52 1.59 1.63 1.68 1.75 1.79 1.87 1.92 1.96 2.03];

OCCEa = [0 21.4 25.04 34.7 45 53.1 67 72.3 84.1 91.6 100 112.9 115.9 122.5 133.7 139.2 142.7
152.7 157.5 ...
165.6 166.4 172.3 176.9 181.7 185.3 190.2 192 194.4 197.9 199.7 203.5 205.9 207.3 210.2];

% SCCIf and SCCIa are laboratory obtained values

SCCIf = [0 0.1 0.125 0.148 0.165 0.19 0.24 0.265 0.295 0.328 0.362 0.394 0.425 0.46 0.486 ...
0.511 0.541 0.562 0.591 0.613 0.635 0.655 0.672 0.699 0.724 0.741];

SCCIa = [0 1.6 2 2.4 2.67 3.12 3.97 4.32 4.84 5.39 6.15 6.61 7.19 7.81 8.24 8.77 9.42 9.61 ...
10.3 10.8 11.1 11.5 12 12.3 13.1 13.4];

% Raw Lab Data plot OCC and SCC
figure(1);
[AX,H1,H2]=plotyy(OCCIf,OCCEa,SCCIf,SCCIa);

% The following code just labels both y axes and sets axis limits

set(get(AX(1),'Ylabel'),'String','E_{\phi\phi} (V_{RMS})');
set(get(AX(2),'Ylabel'),'String','I_{\phin} (A_{RMS})');

% formatting for figure 1

axes(AX(1)) % handle for left axis
axis([0 2.5 0 220]); % This is left y axis range
grid;
axes(AX(2)) % handle for right axis
axis([0 2.5 0 80]); % This is left y axis range
```

```

grid;

xlabel('I_f (A)');

% title('OCC and SCC characteristics');

% OCC fitted curve

% Obtain a linear fit curve and make sure starts at zero therefore mirror about (0,0)

linearx = [-1*OCCIf(10:-1:1) OCCIf(1:10)];
lineary = [-1*OCCEa(10:-1:1) OCCEa(1:10)];

Kagtemp = polyfit(linearx,lineary,1);
Kag = Kagtemp(1);
x1 = [0:.01:1.2];           % Range of values
y1 = x1*Kag;                % Linear y values

ind = 14;                    % ind adjusted until fitted curve matches
last = length(OCCIf);
Bx = log( (OCCIf(last)-OCCEa(last)/Kag)/(OCCIf(ind)-OCCEa(ind)/Kag) ) / (OCCEa(last) -
OCCEa(ind));
Ax = ( OCCIf(last)- OCCEa(last)/Kag )/exp(Bx*OCCEa(last));
Ef1 = 0:.1:210;
If1 = Ef1/Kag + Ax*exp(Bx*Ef1); % See chapter 4 of thesis

figure(2);
plot(OCCIf,OCCEa,If1,Ef1);    % plot laboratory OCC versus fitted OCC
xlabel('I_f (A)');           % label x axis
ylabel('E_{\phi\phi} (V_{RMS})');
axis([0 2.03 0 210.2]);
grid;
% title('I_f = E_{AB}/K_{ag} + A_xe^{B_xE_{AB}}');
text(1.4,80,'K_{ag} = 165','FontSize',18);
text(1.4,60,'A_x = .0023','FontSize',18);
text(1.4,40,'B_x = .0276','FontSize',18);
legend('Lab Data','Fitted Equation');

% SCC fitted curve

linearx = [-1*SCCIf SCCIf(2:length(SCCIf))]; % this mirrors short circuit current about 0,0
lineary = [-1*SCCIa SCCIa(2:length(SCCIf))]; % mirror y about 0,0
% This ensure fitted curve starts at 0,0

KSCC = polyfit(linearx,lineary,1);          % linear fit

```

```

If1 = 0:.001:.741;
Ia = If1 * KSCC(1,1);      % Fitted linear curve for armature current
figure(3);

plot(SCCIf,SCCIa,If1,Ia)  % plot actual versus fitted
grid;

% Graph formatting

xlabel('I_f (A)');
ylabel('I_{\phin} (A_{RMS})');
legend('Lab Data','Linear Fit');
% title('Short Circuit Characteristics (Min Dong)');
text(1,12,'Slope = 17.4 A/A','FontSize',18);

% Xd curve (Xd corresponds to Ia = Irating in SCC

Ef2 = 6:.1:210.2;
If2 = Ef2/Kag + Ax*exp(Bx*Ef2); % See thesis for equation explanation
Ia2 = If2*KSCC(1,1);

Xd = Ef2./Ia2;           % Here is the direct axis reactance over entire range of armature current

figure(4);
plot(If2,Xd);           % Graph formatting
grid;
xlabel('I_f');
ylabel('X_d');

Xdag = Kag/KSCC(1,1);   % Air gap reactance, this is in the linear regions
Irating = 5000/(3*120); % Direct axis reactance for machine is defined at Current rating for
                        % machine
If3 = Irating/KSCC(1,1); % field current corresponding to armature current rating

for temp = 1:length(If2) % Find index of field current corresponding to armature rating
    if If2(temp)<If3
        index = temp;
    end
end
Ef3 = Ef2(index);       % Armature voltage at current rating

Xd = Ef3/Irating;       % Direct Axis reactance at rated armature current

Pb = 5000;              % base power (rating)
Vb = 120*sqrt(3);       % base voltage (rating)

```



```
Zb = Vb^2/Pb;          % Base resistance

xd = Xd/Zb            % per unit direct axis reactance
% title('X_d Ming Dong');
text(1,4,'X_d = 8.70\Omega','FontSize',18);
text(1,3,'X_{dag} = 9.46\Omega','FontSize',18);
text(1,2,'x_d = 1.01 p.u.','FontSize',18);
```

APPENDIX 2 - MATLAB tachometer to frequency code

```
% Speed profile for short circuits
%
% This code requires .MAT files for inputs. These .MAT are obtained from
% the oscilloscope data capture code. The .MAT files necessary are from
% the tachometer output which in our configuration was at the gear to the
% DC motor. The output is the speed profile of the generator.

clear all;

load JAN19_6.mat;          % This was the oscilloscope data capture.
                           % Tachometer data are voltages. Does not matter what oscope
                           % settings are. Voltages are converted in this code to frequency.
tak1 = data(:,1);         % The first column in this case was tachometer.
                           % the variable t is time from oscope.

avg1 = mean(tak1);        % This average will be used to compare hall
                           % output and convert to 0 or 1.

up=0;                      % up and down are counters.
down=0;

for x=1:1:length(t)       % Count hi voltages and low voltages and convert to binary
    if tak1(x) > avg1     % hi voltage converted to 1
        tak1(x) = 1;     % low voltages converted to 0
        up=up+1;
    else
        tak1(x)=0;
        down=down+1;
    end
end

trans1=0;                  % This will count transitions from 0 to 1 and vice
                           % versa
arry1 = [];                % This will contain the times at each transition.
                           % As well as Hi or Low.

for x=1:1:length(t)-1
    if tak1(x)-tak1(x+1)~=0
        arry1 = [arry1;t(x) tak1(x);t(x+1) tak1(x+1)];
        trans1 = trans1+1;
    end
end
```

```

cycles = trans1/32;    % total number of electrical cycles for generator
                    % during oscscope data capture. Just informational.

frq1=[];                % This will hold mid point times and frequencies.

for x=2:4:length(arry1)-5
    frq1 = [frq1;arry1(x,1)+((arry1(x+3,1)-arry1(x,1)))/2 1/12*(12/32)*...
            (12/14)*2/(arry1(x+3,1)-arry1(x,1))];
end

pa = polyfit(frq1(:,1),frq1(:,2),12);    % Fit a curve to frequency data.

ta = .00001:.00001:.1;
f3 = 2*pi*polyval(pa,ta);

% This plots real time frequency and fitted curve.
figure(1)
plot(frq1(:,1),frq1(:,2),ta,f3/2/pi);
grid;
ylim([35 65]);

save dcmotorspeed.mat frq1;            % Save for use by simulation.

```

APPENDIX 3 – MATLAB Bench Generator Model Code

```
% Synchronous Generator Simulation
% Using Notes from Professor Kirtley's Class 6.685
% Also using solution set for PS 11 of same class
% Uses mi.m, miq.m, and sf2.m functions

clear all;
clear figures;
global ydd ydk ykd ydf yff yqq yqk ykf ykq rf rkd rkq omz ra r1 vf...
    H Tm zx endfreq transientlength ct1 Ifprofile

%%%%%%%%%%%%%%
%      INPUTS      %
%%%%%%%%%%%%%%

% Unknown Values - Will need to match to simulation

xd = 1.0069;      % synchronous d- axis reactance
xq = .770486;    % synchronous q- axis reactance
xdp = .19676;    % transient (d-axis) reactance
xdpp = .094;     % subtransient d- axis reactance
xqpp = .15;      % subtransient q- axis reactance
tdop = .4088;   % transient (open circuit) time constant
tdopp = .03;    % subtransient d- axis time constant
tqopp = .07;    % subtransient q- axis time constant
xl = .05;       % armature leakage reactance
H = .19;        % rotor inertia

% Known Values

omz = 60*2*pi;   % base frequency
Pb = 5000;       % base power (rating)
Vb = 120;        % base voltage (rating) line to neutral
                % We are 208 line to line
Zb = Vb^2/Pb*3;  % Impedance Base
Ib=Pb/Vb/3;     % Current Base

%p=2;           % Not used % number of pole pairs
%r1=2592        % 1296 Ohms = 100W, 2592 Ohms = 50W
                % r1 used if not doing short circuit
                % This was used in early bench testing with resistor values used in lieu of
                % shorts

t0 = 0;         % Simulation Start Time (seconds)
```

```

tf = .08;           % Simulation Stop Time
[xad xkdl xfl rkd rf] = mi(xd, xdp, xdpp, ttop, tdopp, xl, omz); % Determine direct axis model
                                                    % parameters

Ifb=2;             % Field Current Base
Vfb=3*Vb*Ib/Ifb;  % Field Voltage Base
Zfb=Vfb/Ifb;      % Field Resistance Base

rf=15.8/Zfb;      % Use this measured resistance ilo calc rf in mi.m convert to per unit

xkd = xad + xkdl;  % Based on circuit model
xf = xad + xfl;   % Based on circuit model
xmd = [xd xad xad; xad xkd xad; xad xad xf]; % direct axis reactance 3x3 matrix (equal
                                                    % mutuals model)

ymd = inv(xmd);
[xaq xkql rkql] = miq(xq, xqpp, tqopp, xl, omz); % quadrature axis parameters
xkq = xaq + xkql; % q-axis damping
xmql = [xq xaq; xaq xkql]; % 2x2 matrix in equal mutuals model
ymql = inv(xmql);

ydd = ymd(1,1);   % inverted xmd matrix parameters
ydk = ymd(1,2);
ykd = ymd(2,2);
ydf = ymd(1,3);
yff = ymd(3,3);
ykf = ymd(2,3);
yqq = ymql(1,1);
yqk = ymql(1,2);
yqk = ymql(2,2);

ra = .48/Zb;      % Measured value (use this one)

vf = 31/Vfb       % Measured vf to get to rated voltage (use this one)
Tm = 0;           % Open circuit voltage therefore zero Mechanical Torque

% psi0 = [psid0 psiq0 psikd0 psikq0 psif0 om0]
psi0 = [1 0 1 0 1+xfl/xad omz];

dt = 1/8024;      % Simulation step size
time = t0:dt:tf;  % Time of simulation

load if0.mat;     % This is real field current from short circuit test
                  % This is obtained from oscscope.

% figure(1)
% plot(Ifprofile(:,1)*1000,Ifprofile(:,2));

```

```

% xlabel('Time (ms)');
% ylabel('Field Current (per unit)');
% grid;

[t,psi] = ode45('sfMD',time, psi0);           % sfMD.m file

id = ydd .* psi(:,1) + ydk .* psi(:,3) + ydf .* psi(:,5);   % direct axis current
iq = yqq .* psi(:,2) + yqk .* psi(:,4);                     % quadrature axis current

Ib = Pb/(3*Vb);                                           % Current to neutral 13.89 A

a = 2*pi/3;
omz = psi(:,6);                                           % omega profile factoring in inertia

ia = sqrt(2)*Ib*(id .* cos(omz.*t) - iq .* sin(omz.*t));
ib = sqrt(2)*Ib*(id .* cos(omz.*t - a) - iq .* sin(omz.*t - a));
ic = sqrt(2)*Ib*(id .* cos(omz.*t + a) - iq .* sin(omz.*t + a));
iff = ydf .* psi(:,1) + ykf .* psi(:,3) + yff .* psi(:,5);
ikd = ydk .* psi(:,1) + ykd .* psi(:,2) + ykf .* psi(:,3);

figure(2);
plot(t*1000,ia,t*1000,ib,t*1000,ic);           % Line to neutral currents
title('Fault Current, SHORT CIRCUIT Simulation');

xlim([0 80])
ylim([-200 200])
ylabel('I_{\phi-n} (A)');
xlabel('Time (ms)');
legend('i_a','i_b','i_c');
grid

```

MI.M

```

% model elements from terminal parameters mi.m
function [xad, xkd, xf, rkd, rf] = mi(xd, xdp, xdpp, tdop, tdopp, xl, omz)
xad = xd - xl;
xf = xad * (xdp - xl) / (xad - xdp + xl);
xkd = 1/(1/(xdpp-xl) - 1/xad -1/xf);
rf = (xf)/(omz * tdop);
rkd = (xkd + xad*xf/(xad +xf))/(omz*tdopp);

```

MIQ.M

```

% model elements from terminal parameters miq.m
function [xaq, xkq, rkq] = miq(xq, xqpp, tqopp, xl, omz)
xaq = xq -xl;

```

```

xkq = xaq*(xqpp -xl)/(xaq-xqpp+xl);
rkq = (xaq+xkq)/(omz*tqopp);

```

SF2.M

```
function dpsi = sf2(t,psi)
```

```
global ydd ydk ykd ydf yff yqq yqk ykf ykq rf rkd rkq omz ra r1 vf H Tm zx...
endfreq transientlength w0 Ifprofile frq1
```

```

psid = psi(1);
psiq = psi(2);
psikd = psi(3);
psikq = psi(4);
psif = psi(5);
om = psi(6);

```

```

index = t/Ifprofile(end,1)*length(Ifprofile);           % Used to index to actual
                                                         % field current

```

```

id = ydd*psid + ydk*psikd + ydf*psif;
ikd = ydk* psid + ykd*psikd + ykf*psif;

```

```

iff=Ifprofile(round(index)+1,2);                         % Actual Field Current Data

```

```

iq = yqq * psiq + yqk* psikq;
ikq = yqk * psiq + ykq* psikq;

```

```
te = psid*iq - psiq *id;
```

```
%%%%%%%%%
```

```

psidot1 = om*(psiq) - omz*(ra)*id ;
psidot2 = -om*psid - omz*(ra)*iq;
psidot3 = -omz*rkd*ikd;
psidot4 = -omz*rkq*ikq;
psidot5 = omz*vf - omz*rf*iff;

```

```
omdot = (omz/(2*H))*(te + Tm);
```

```
dpsi = [psidot1 psidot2 psidot3 psidot4 psidot5 omdot]';
```

PLOTSHORT.M

```
% plotshort.m
% This m file determines xdp and xdpp by plotting classical equation versus % % oscilloscope
output. Also determines Tdp and Tdpp.

clear all

load w6inertia_JAN19.mat; % radial speed profile from JAN19_6.mat
wreal=f3; % f3 is from w6inertia_JAN19.mat
% This is used in classical equation

load JAN19_6.mat; % channel 1 is tachometer
% Channel 2 is Vswitch
% Channel 3 is Field Current
% Channel 4 is Short circuit Current

V = 120*sqrt(2); % used for classical plot Voltage to neutral

delay = pi/180*200; % Match classical phase to oscope and
% simulation. Purely to make sine waves be on
% same phase (visually).

Xd = 8.7; % Known value. See Appendix I.

% Xdp, Xdpp, Tdp, and Tdpp are estimated from this program (trial and
% error)

Xdp = 1.7; % Match Xdp, Xdpp, Tdp, and Tdpp to oscope data
Xdpp = .81216;
Tdp = 45e-3;
Tdpp = 15e-3;

ib = []; % Capture classical equation current

t0=18.3e-3; % When current starts (match delay from oscope to
% classical equation). When switch turned on.

% t0 is based on looking at oscilloscope real data. When does short start.

for x=1:1:length(t)
```



```

if t(x) < t0      % Ib ILO Vswitch activated since not at same time
    ib = [ib;0];
else
    ib = [ib;V*(1/Xd + (1/Xdp -1/Xd)*exp(-(t(x)-t0)/Tdp) + (1/Xdpp - 1/Xdp)*exp(-(t(x)-
t0)/Tdpp))...
        *sin(wreal(x)*t(x)-delay)];
end
end
end

```

```

figure(3);
plot((t)*1000-18.3,data(:,4)*1000,(t)*1000-18.3,ib,simdata(:,1),simdata(:,2),t*1000,-
ones(length(t),1)*threshold);
ylim([-200 200]);

```

```

grid;
xlim([0 50]);
xlabel('Time (ms)');
ylabel('I_{\phin} (A)');
legend('I_{\phin} FLUKE','I_{\phin} Classical','I_{\phin} Simulation');
title('Short Circuit Current');

```

APPENDIX 4 – MATLAB DDG-51 Simulation Code and DDG-II Results

```
% DDG Simulation
% This code uses inputs from NAVSEA to simulate a three phase symmetrical % % % short

clear all;

global ydd r1 ydk ykd ydf yff yqq yqk ykf ykq rf rkd rkq omz ra vf Tm H delta

% DDG generator 1

Pb = 3125e3;
Vb = 450/sqrt(3);    % line to neutral

Zb = Vb^2/Pb*3;      %
Ib=Pb/Vb/3;
pf = .8;
p = 2;
H = 2.137;
ra = .00515;
xl = .08;

xaq = 1;
rkq = .0613;
xkql = .329787;

xad = 1.768;
rf = .00111;
xfl = .136829;
rkd = .023968;
xkdl = .333829;

% Calculations to determine other parameters

xq = xaq + xl;
xd = xad + xl;

xkq = xaq + xkql;

xqpp = xl + (xaq*xkql)/(xkql + xaq);

xdp = xl + (xad*xfl)/(xad + xfl);

xdpp = 1/(1/xad + 1/xkdl + 1/xfl)+ xl;
```

```

omz = 2*pi*60;
xf = xad + xfl;
xkd = xad + xkdl;

tdop = 1/(omz*rf)*(xfl + xad)+1/(omz*rkd)*(xkdl + xad);

tqopp = 1/(omz*rkq)*(xkq + xaq);
tdopp = 1/(omz*rkd)*(xkdl + (xad*xfl)/(xad + xfl))...
/(1 + (1/(omz*rkd)*(xkdl + (xad*xfl)/(xad + xfl)))/(1/(omz*rf)*(xfl + (xad*xfl)/(xad + xfl))));

tdp = 1/(omz*rf)*(xfl + (xad*xl)/(xad + xl)) + 1/(omz*rkd)*(xkdl + (xad*xl)/(xad + xl));

tdpp = 1/(omz*rkd)*(xkdl + (xad*xfl*xl)/(xad*xfl + xad*xl + xfl*xl))...
/(1 + (1/(omz*rkd)*(xkdl + (xad*xl)/(xad + xl)))/(1/(omz*rf)*(xfl + (xad*xl)/(xad + xl))));

% Initial conditions

vt = 1; % terminal voltage
ia = 0; % terminal current magnitude
psi1 = acos(.8); % power factor angle
i_a = ia*(pf - j*sin(psi1)); % as a complex vector
v_i = vt + ra*i_a; % this is the internal voltage vector
vi = abs(v_i); % and this is the absolute value of
% internal voltage
ai = angle(v_i); % and this is the angle of the internal
% voltage
e_1 = v_i + j*i_a*xq; % the voltage that defines the q axis
e1 = abs(e_1);
delta = angle(e_1); % and this is the phase angle
id = ia*sin(delta + psi1); % this is direct axis current
iq = ia*cos(delta + psi1); % and this is quadrature axis current
vq = vi*cos(delta - ai); % q axis component of that internal
% voltage
vd = vi*sin(delta - ai); % d axis component
eaf = vq + id*xd; % voltage behind synchronous reactance
i_f = eaf/xad; % steady field current
vf = i_f*rf; % exciter voltage
psid0 = vq; % fluxes are -90 degrees rotated from
% internal voltage
psiq0 = -vd;
psikd0 = psid0 + id*xl; % same as flux on the magnetizing
% inductance
psikq0 = psiq0 + iq*xl; % this is the same too
psif0 = psikd0 + xfl*i_f; % flux initial condition

Tm = psid0*iq - psiq0*id; % generating torque

```

```

psia = [psid0 psiq0 psikd0 psikq0 psif0 omz];
xmd = [xd xad xad; xad xkd xad; xad xad xf];
ymd = inv(xmd);

xmq = [xq xaq; xaq xkq];
ymq = inv(xmq);
ydd = ymd(1,1);
ydk = ymd(1,2);
ykd = ymd(2,2);
ydf = ymd(1,3);
yff = ymd(3,3);
ykf = ymd(2,3);
yqq = ymq(1,1);
yqk = ymq(1,2);
ykq = ymq(2,2);

% END INITIAL CONDITIONS

time = -.05:1/2024:-1/2024;          % negative values used to annotate pre-fault

[tp,psip] = ode45('sf1',time, psia);

idp = ydd .* psip(:,1) + ydk .* psip(:,3) + ydf .* psip(:,5);
iqp = yqq .* psip(:,2) + yqk .* psip(:,4);

% psi0 = [psid0 psiq0 psikd0 psikq0 psif0 omz0]
psi0 = [psip(end,1) psip(end,2) psip(end,3) psip(end,4) psip(end,5) omz];

t0 = 0;
tf = .50;

% psi0 = [psid0 psiq0 psikd0 psikq0 psif0 omz];
dt = (tf-t0)/2024;

time = t0:dt:tf;
[t,psi] = ode45('sf2',time, psi0);

id = ydd .* psi(:,1) + ydk .* psi(:,3) + ydf .* psi(:,5);
iq = yqq .* psi(:,2) + yqk .* psi(:,4);
te1 = (psi(:,1).*iq - psi(:,2).*id);

id = [idp;id];
iq = [iqp;iq];

```

```

t= [tp;t];

a = 2*pi/3;
oma = [psip(:,6);psi(:,6)];
ia = id .* cos(oma.*t) - iq .* sin(oma.*t);
ib = id .* cos(oma.*t - a) - iq .* sin(oma.*t - a);
ic = id .* cos(oma.*t + a) - iq .* sin(oma.*t + a);
iff = ydf .* psi(:,1) + ykf .* psi(:,3) + yff .* psi(:,5);
ikd = ydk .* psi(:,1) + ykd .* psi(:,2) + ykf .* psi(:,3);

threshold = Ib*sqrt(2)*ones(length(t),1);

figure(1)
clf
Ib = Pb/(3*Vb);
plot(t*1000, ia*Ib/1000*sqrt(2), t*1000, ib*Ib/1000*sqrt(2), t*1000, ic*Ib/1000*sqrt(2), t*1000, threshold*1.5/1000);
% title('Fault Current DDG');
ylabel('I_{line} (KA)');
xlabel('Time, ms');
xlim([-50 500]);
grid on;
legend('I_A','I_B','I_C');

imax=max(ic*Ib);

% figure(2);
% subplot 211
% plot(t, iq*Ib);grid;
% title('I_q and I_d');
% subplot 212
% plot(t,id*Ib);grid;
% xlabel('Time (seconds)');

figure(3)
plot(t*1000,oma/omz*60);grid;
xlabel('Time (ms)');
ylabel('Frequency (Hz)');

% Ifb = 1.5*Vb*Ib/vf;
% figure(4)
% plot(t, iff*Ib);grid;
%
```

```

% figure(5);
% Tb = .0658e6*omz/(2*H);
% plot(t,te1*Tb);grid;
%
% figure(6);
% plot(t,psi(:,7)/pi*180);grid;

```

DDG II Simulation – These are simulation results using DDG-II parameters from Chapter 5
 (Note that code above shows DDG-I parameters)

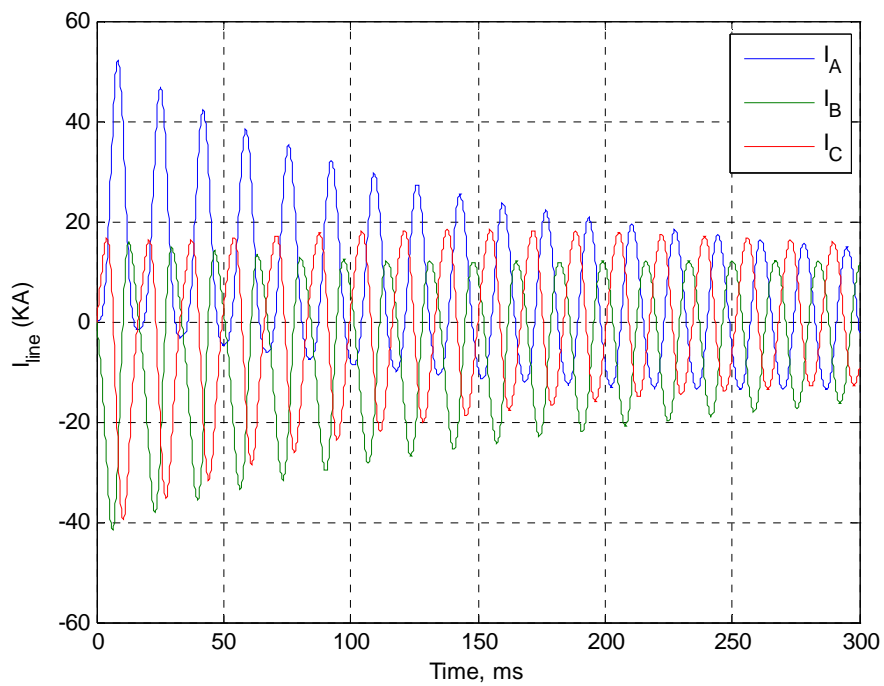


Figure 34: DDG-II Short Circuit Simulation (Initially Unloaded)

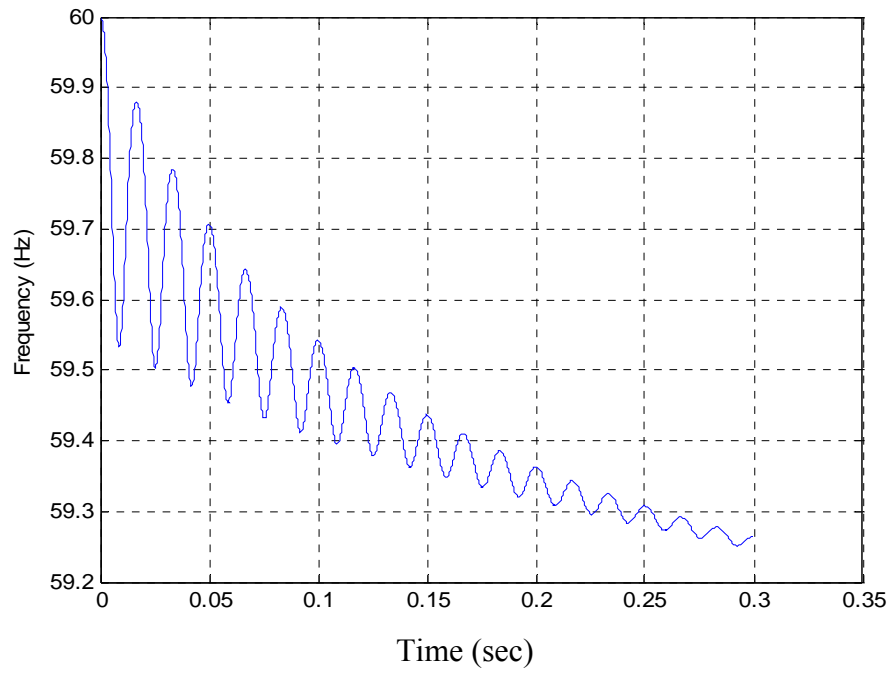


Figure 35: DDG-II Short Circuit Simulation Frequency Response (Initially Unloaded)

APPENDIX 5 – SIMULATION USERS GUIDE

All data files and simulation code is located on the bucket account under leghorn.

Bench Generator Simulation Notes

PLOTSHORT.M

1. Plotshort.m file is used to determine the short circuit transient and sub-transient reactances and time constants. $(X'_d, X''_d, T'_d, T''_d)$
2. These inputs are entered based on some assumptions. The assumptions for the generator being tested were that the transient reaction was dominant compared to sub-transient reaction. Therefore the initial matching technique was to assume zero sub-transient reaction and match transient parameters as best as possible. Next match sub-transient parameters.
3. The speed profile used in the classical equation was obtained from the tachometer results which were a .MAT file from Appendix 2 code. Alternatively the speed profile from the simulation can be used since this is ultimately matched to the tachometer frequency.

MDSIMULATION.M

1. The functions used by this simulation are MI.M, MIQ.M, and SFMD.M.
2. MI.M calculates direct axis parameters.
3. MIQ.M calculates quadrature axis parameters.
4. SFMD.M is the function used by ode45 and is based on the equal mutuals model.
5. SFMD.M uses actual data for field current. This is what the Ifprofile parameter is. Field current is calculated for the DDG simulations.
6. The rotor inertia constant (H) is determined by matching the simulation frequency response to the actual generator slow down. The larger H is the less slowdown will be seen in the simulation.

7. The armature leakage reactance is somewhat arbitrary but it is important to make sure that none of the equal mutuals parameters are negative as a result of this value. Typical range of leakage reactance is 0.04 - 0.15.
8. There are typical ranges of values for $(x_q, x_q'', t'_{do}, t''_{do}, \text{ and } t''_{qo})$ (11)(9). These are used in conjunction with the values obtained in plotshort.m for an initial estimate. The sensitivity analysis conducted in chapter 5 should be looked at to determine the parameters that need to be adjusted carefully.
9. The simulation can now be adjusted to match the actual oscilloscope results.
10. If0.mat is the actual field current data from the oscilloscope.
11. Initial conditions can be entered by adjusting ia. For open circuited initially this is set to zero and for fully loaded this is set to one. Any other loading condition can be entered also.
12. The DDG simulation does not require MI.M or MIQ.M since all the parameters can be directly calculated without those functions.

APPENDIX 6 – MATLAB MODEL VERIFICATION

The MATLAB model employed for this thesis was used to run the simulation of a three phase fault using the parameters shown in Figure 36. The actual results are shown in Figure 37. The simulation model employed and the results from that simulation are shown below. There are no specific values to be compared but the envelopes from each of the graphs (Figure 38 - Figure 40) match the Krause results. Also the magnitudes match. Based on the matching results the equal mutuals simulation model is validated. It should be noted that since there were two quadrature axis damper windings provided in the data in Figure 36 the equal mutuals model was modified to account for the second damper winding. This also shows that if the bench generator is modeled with more than one damper winding this can easily be adapted into the simulation code.

Table 5.10-2 Steam turbine generator	
Rating: 835 MVA	
Line to line voltage: 26 kV	
Power factor: 0.85	
Poles: 2	
Speed: 3600 r/min	
Combined inertia of generator and turbine: $J = 0.0658 \times 10^6 \text{ J}\cdot\text{s}^2$, or $WR^2 = 1.56 \times 10^6 \text{ lbm}\cdot\text{ft}^2$ $H \approx 5.6 \text{ s}$	
Parameters in ohms and per unit:	
$r_s = 0.00243 \ \Omega, 0.003 \text{ pu}$	
$X_{is} = 0.1538 \ \Omega, 0.19 \text{ pu}$	
$X_{q1} = 1.457 \ \Omega, 1.8 \text{ pu}$	$X_d = 1.457 \ \Omega, 1.8 \text{ pu}$
$r'_{kq1} = 0.00144 \ \Omega, 0.00178 \text{ pu}$	$r'_{fd} = 0.00075 \ \Omega, 0.000929 \text{ pu}$
$X'_{lkq1} = 0.6578 \ \Omega, 0.8125 \text{ pu}$	$X'_{lfd} = 0.1145 \ \Omega, 0.1414 \text{ pu}$
$r'_{kq2} = 0.00681 \ \Omega, 0.00841 \text{ pu}$	$r'_{kd} = 0.01080 \ \Omega, 0.01334 \text{ pu}$
$X'_{lkq2} = 0.07602 \ \Omega, 0.0939 \text{ pu}$	$X'_{kd} = 0.06577 \ \Omega, 0.08125 \text{ pu}$

Figure 36: Krause Simulation used to verify Equal Mutuals Simulation Model

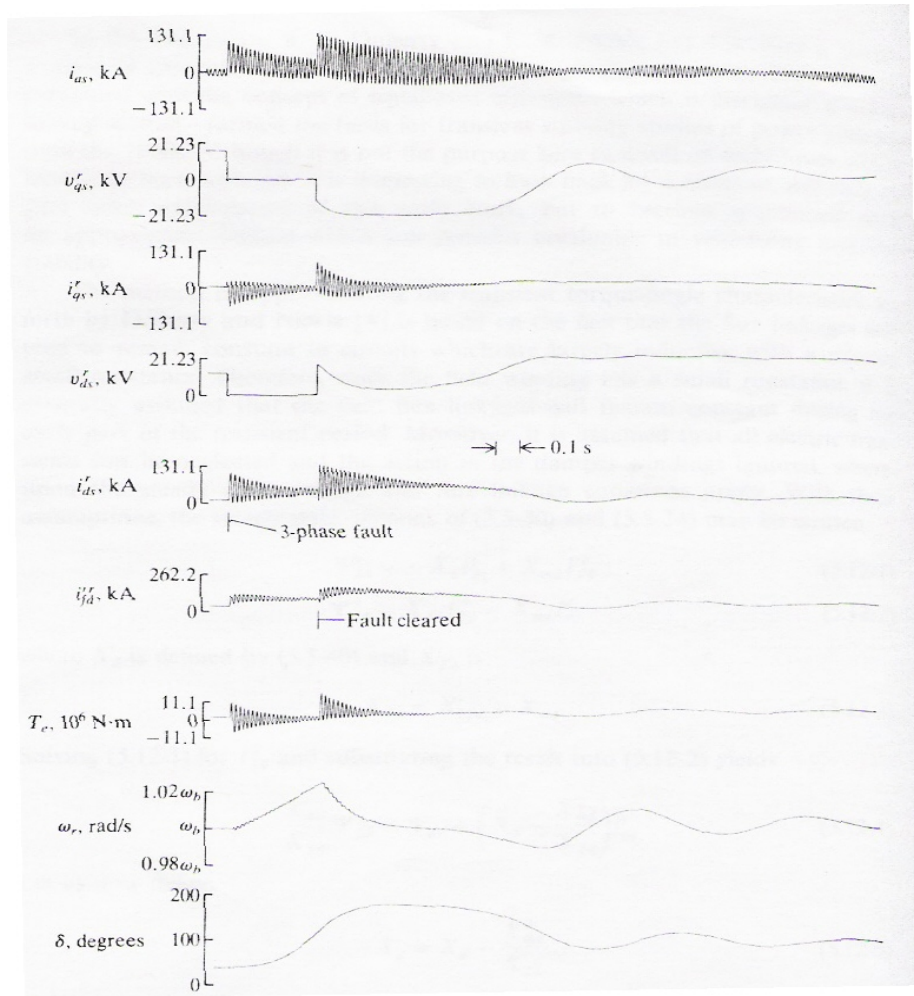


Figure 37: Krause Simulation Results

% Krause Simulation from Chapter 5
 % This was used to validate our model. Known inputs were entered into the
 % simulation and the results matched known outputs. These were provided
 % from "Analysis of Electric Machinery". See Bibliography.

clear all;

global ydd ydk ykd ydf yff yqq yqk1 yqk2 ykf ykq1 ykq2 y3 rf rkd rkq1 rkq2 omz ra vf Tm H

Chap5params;

ta = .5*(xdpp+xqpp)/(omz*ra);

t0 = 0;

tf = .362;

xmd = [xd xad xad; xad xkd xad; xad xad xf];

```

ymd = inv(xmd);

xmq = [xq xaq xaq; xaq xkq1 xaq; xaq xaq xkq2];
ymq = inv(xmq);
ydd = ymd(1,1);
ydk = ymd(1,2);
ykd = ymd(2,2);
ydf = ymd(1,3);
yff = ymd(3,3);
ykf = ymd(2,3);

yqq = ymq(1,1);
yqk1 = ymq(1,2);
yqk2 = ymq(1,3);
ykq1 = ymq(2,2);
ykq2 = ymq(3,3);
y3 = ymq(2,3);

% flux vector is [psid psiq psikd psikq psif]

psi0 = [psid0 psiq0 psikd0 psikq1 psif0 omz psi1 psikq2];

dt = (tf-t0)/1024;
Tm = .852; % added from chapt 5
time = t0:dt:tf;
[t,psi] = ode45('sf',time, psi0);

id = ydd .* psi(:,1) + ydk .* psi(:,3) + ydf .* psi(:,5);
iq = yqq .* psi(:,2) + yqk1 .* psi(:,4) + yqk2 .* psi(:,8);

te1 = (psi(:,1)).*iq - psi(:,2).*id;

a = 2*pi/3;
oma = psi(:,6);
ia = id .* cos(oma.*t) - iq .* sin(oma.*t);
ib = id .* cos(oma.*t - a) - iq .* sin(oma.*t - a);
ic = id .* cos(oma.*t + a) - iq .* sin(oma.*t + a);
iff = ydf .* psi(:,1) + ykf .* psi(:,3) + yff .* psi(:,5);
ikd = ydk .* psi(:,1) + ykd .* psi(:,2) + ykf .* psi(:,3);

% open circuit out of phase

psi0 = psi;
% psi0 = [0 0 0 0 1+xfl/xad];
t01 = .36201;

```

```

tf1 = 2.4;
dt = (tf1-t01)/1024;

time1 = t01:dt:tf1;
psi(end,7)

[ta,psia] = ode45('sf1',time1, psi(end,:));

ida = ydd .* psia(:,1) + ydk .* psia(:,3) + ydf .* psia(:,5);
iqa = yqq .* psia(:,2) + yqk1 .* psia(:,4)+ yqk2*psi(:,8);

te2 = -(psia(:,1).*iqa - psia(:,2).*ida);

a = 2*pi/3;
oma = psi(:,6);
ia1 = ida .* cos(oma.*ta) - iqa .* sin(oma.*ta);
ib1 = ida .* cos(oma.*ta - a) - iqa .* sin(oma.*ta - a);
ic1 = ida .* cos(oma.*ta + a) - iqa .* sin(oma.*ta + a);
iff1 = ydf .* psia(:,1) + ykf .* psia(:,3) + yff .* psia(:,5);
ikd1 = ydk .* psia(:,1) + ykd .* psia(:,2) + ykf .* psia(:,3);

% group terms

ia = [ia; ia1];
ib = [ib; ib1];
ic = [ic; ic1];
iff = [iff; iff1];
ikd = [ikd; ikd1];
t = [t; ta];
te1 = [te1; te2];
psi = [psi; psia];
id = [id; ida];
iq = [iq; iqa];

figure(1)
clf
subplot 311
Ib = Pb/(sqrt(3)*Vb);
plot(t, -ib*Ib),%, t, ib, t, ic);
title('Fault Current');
ylabel('I_{\phi} (A)');

grid on;

imax=max(ic*Ib)

```

```

subplot 312
plot(t, -iq*Ib);grid;
ylabel('I_q (A)');
subplot 313
plot(t,-id*Ib);grid;
xlabel('Time, s');
ylabel('I_d (A)');

```

```

figure(2)
subplot 211
plot(t,psi(:,6)/omz);grid;
ylabel('\omega (per unit)');
subplot 212
plot(t,psi(:,7)/pi*180);grid;
ylabel('\theta (degrees)');
xlabel('Time (sec)');

```

```

figure(3)
subplot 211
plot(t, iff*Ib);grid;
ylabel('Field Current (A)');

```

```

subplot 212
Tb = .0658e6*omz/(2*H);
plot(t,te1*Tb);grid;
ylabel('Torque (Nm)');
xlabel('Time (sec)');

```

CHAP5PARAMS.M

% Parameters for Chapter 5 Simulation:

```

Pb = 835e6;
Vb = 26e3;
Zb = Vb^2/Pb;
pf = 0.85;
p = 1;          % Number of pole pairs
H = 5.6;

ra = .003;
xl = .19;

```

```

xq = 1.8;
rkq1 = .00178;
xlkq1 = .8125;
rkq2 = .00841;
xlkq2 = .0939;

xkql = imag((rkq1 + j*(xlkq1))*(rkq2 + j*(xlkq2))/((rkq1 + j*(xlkq1)) + (rkq2 + j*(xlkq2))));
rkq = real((rkq1 + j*(xlkq1))*(rkq2 + j*(xlkq2))/((rkq1 + j*(xlkq1)) + (rkq2 + j*(xlkq2))));

xd = 1.8;
rf = .000929;
xfl = .1414;
rkd = .01334;
xkdl = .08125;

xaq = xq - xl;
xad = xd - xl;

xkq = xaq + xkql;
xkq1 = xaq + xlkq1; % Added
xkq2 = xaq + xlkq2; % Added

xqp = xl + (xaq*xlkq1)/(xlkq1 + xaq);
xdp = xl + (xad*xfl)/(xad + xfl);

xqpp = xl + (xaq*xlkq1*xlkq2)/(xaq*xlkq1 + xaq*xlkq2 + xlkq1*xlkq2);
xdpp = xl + (xad*xfl*xkdl)/(xad*xfl + xad*xkdl + xfl*xkdl);

omz = 2*pi*60;

tdop = 1/(omz*rf)*(xfl + xad)+1/(omz*rkd)*(xkdl + xad);

tqopp = 1/(omz*rkq2)*(xlkq2 + (xaq*xlkq1)/(xlkq1 + xaq))...
/(1 +(1/(omz*rkq2)*(xlkq2 + xaq))/(1/(omz*rkq1)*(xlkq1 + (xaq))));
tdopp = 1/(omz*rkd)*(xkdl + (xad*xfl)/(xad + xfl))...
/(1 +(1/(omz*rkd)*(xkdl + (xad)))/(1/(omz*rf)*(xfl + (xad))));

tqp = 1/(omz*rkq1)*(xlkq1 + (xaq*xl)/(xl + xaq))+1/(omz*rkq2)*(xlkq2 + (xaq*xl)/(xl + xaq));

tdp = 1/(omz*rf)*(xfl + (xad*xl)/(xad + xl)) + 1/(omz*rkd)*(xkdl + (xad*xl)/(xad + xl));

```

```
tqpp = 1/(omz*rkq2)*(xlkq2 + (xaq*xlkq1*xl)/(xaq*xl + xaq*xlkq1 + xl*xlkq1))...
/(1 +(1/(omz*rkq2)*(xlkq2 + (xaq*xl)/(xaq + xl)))/(1/(omz*rkq1)*(xlkq1 + (xaq*xl)/(xaq +
xl))));
```

```
tdpp = 1/(omz*rkd)*(xkdl + (xad*xfl*xl)/(xad*xfl + xad*xl + xfl*xl))...
/(1 +(1/(omz*rkd)*(xkdl + (xad*xl)/(xad + xl)))/(1/(omz*rf)*(xfl + (xad*xl)/(xad + xl))));
xf = xad + xfl; %
xkd = xad + xkdl;
```

% Initial conditions

```
vt = 1; % terminal voltage
ia = 1; % terminal current magnitude
psi1 = acos(pf); % power factor angle
i_a = ia*(pf - j*sin(psi1)); % as a complex vector
v_i = vt + ra*i_a; % this is the internal voltage vector
vi = abs(v_i); % and this is the absolute value of internal voltage
ai = angle(v_i); % and this is the angle of the internal voltage
e_1 = v_i + j*i_a*xq; % the voltage that defines the q axis
e1 = abs(e_1);
delta = angle(e_1); % and this is the phase angle
id = ia*sin(delta + psi1); % this is direct axis current
iq = ia*cos(delta + psi1); % and this is quadrature axis current
vq = vi*cos(delta - ai); % q axis component of that internal voltage
vd = vi*sin(delta - ai); % d axis component
eaf = vq + id*xd; % voltage behind synchronous reactance
i_f = eaf/xad; % steady field current
vf = i_f*rf; % exciter voltage
psid0 = vq; % fluxes are -90 degrees rotated from internal voltage
psiq0 = -vd;
psikd0 = psid0 + id*xl; % same as flux on the magnetizing inductance
psikq1 = psiq0 + iq*xl; % this is the same too
psikq2 = psiq0 + iq*xl;
psif0 = psikd0 + xfl*i_f; % flux initial condition

Tm = psid0*iq - psiq0*id % generating torque
```

SF.M

```
function dpsi = sf(t,psi)
global ydd ydk ykd ydf yff yqq yqk1 yqk2 ykf ykq1 ykq2 y3 rf rkd rkq1 rkq2 omz ra vf H Tm%
xd xf xkd xad xaq xq xkq ymd
```

```
psid = psi(1);
psiq = psi(2);
```



```

psikd = psi(3);
psikq1 = psi(4);
psif = psi(5);
om = psi(6);
delta = psi(7);
psikq2 = psi(8);

```

```

id = ydd*psid + ydk*psikd + ydf*psif;
ikd = ydk* psid + ykd*psikd + ykf*psif;
iff = ydf*psid + ykf*psikd + yff*psif;

```

```

iq = yqq * psiq + yqk1 * psikq1 + yqk2*psikq2;
ikq1 = yqk1 * psiq + ykq1* psikq1 +y3 * psikq2 ;
ikq2 = yqk2*psiq + y3*psikq1 + ykq2 * psikq2;

```

```

te = psid*iq - psiq*id;

```

```

psidot1 = om*psiq - omz*ra*id;
psidot2 = -om*psid - omz*ra*iq;
psidot3 = -omz*rkd*ikd;
psidot4 = -omz*rkq1*ikq1;
psidot5 = omz*vf - omz*rf*iff;
omdot = (omz/(2*H))*(Tm+te);
ddot = om-omz;
psidot8 = -omz*rkq2*ikq2;

```

```

dpsi = [psidot1 psidot2 psidot3 psidot4 psidot5 omdot ddot psidot8]';

```

SF1.M

```

function dpsi = sf(t,psi)
global ydd ydk ykd ydf yff yqq yqk1 yqk2 ykf ykq1 ykq2 y3 rf rkd rkq1 rkq2 omz ra vf H Tm%
xd xf xkd xad xaq xq xkq ymd

```

```

psid = psi(1);
psiq = psi(2);
psikd = psi(3);
psikq1 = psi(4);
psif = psi(5);
om = psi(6);
delta = psi(7);
psikq2 = psi(8);

```

```

id = ydd*psid + ydk*psikd + ydf*psif;
ikd = ydk* psid + ykd*psikd + ykf*psif;

```

$$iff = ydf*psid + ykf*psikd + yff*psif;$$

$$iq = yqq * psiq + yqk1 * psikq1 + yqk2 * psikq2;$$

$$ikq1 = yqk1 * psiq + ykq1 * psikq1 + y3 * psikq2 ;$$

$$ikq2 = yqk2 * psiq + y3 * psikq1 + ykq2 * psikq2;$$

$$te = psid*iq - psiq*id;$$

$$psidot1 = om*psiq - omz*ra*id + omz*\sin(\delta);$$

$$psidot2 = -om*psid - omz*ra*iq + omz*\cos(\delta);$$

$$psidot3 = -omz*rkd*ikd;$$

$$psidot4 = -omz*rkq1*ikq1;$$

$$psidot5 = omz*vf - omz*rf*iff;$$

$$omdot = (omz/(2*H))*(Tm+te);$$

$$ddot = om-omz;$$

$$psidot8 = -omz*rkq2*ikq2;$$

$$dpsi = [psidot1 \ psidot2 \ psidot3 \ psidot4 \ psidot5 \ omdot \ ddot \ psidot8]';$$

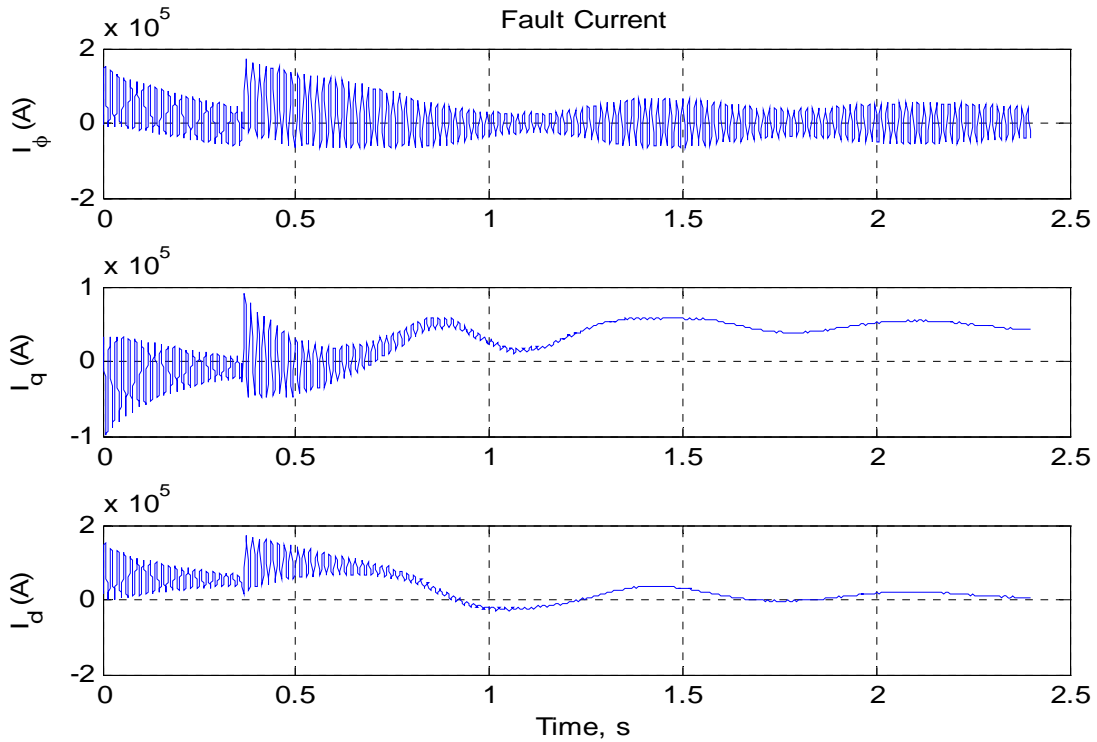


Figure 38: Equal Mutuels Model Results for Krause Simulation (Phase, Direct, and Quadrature Currents)

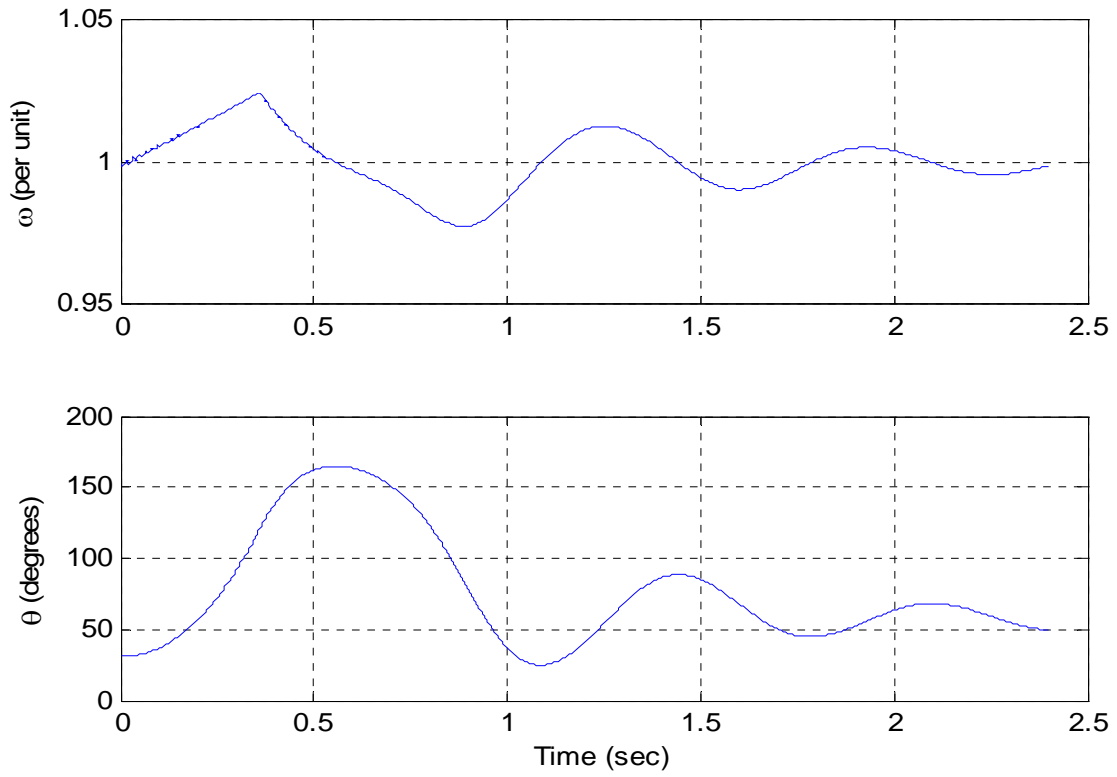


Figure 39: Equal Mutuals Model Results for Krause Simulation (Frequency and Degrees)

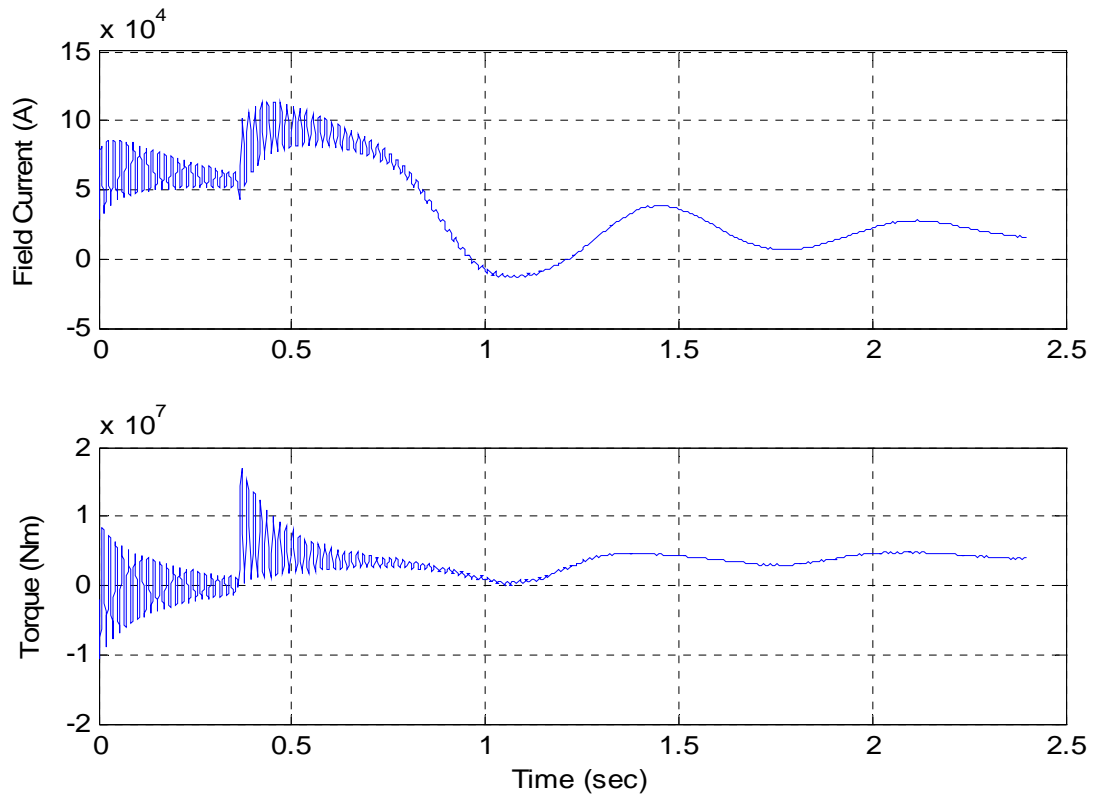


Figure 40: Equal Mutuals Model Results for Krause Simulation (Field Current and Torque)

APPENDIX 7 – CALCULATION OF NAVSEA DDG PARAMETERS

	DDG-I	DDG-II
P_{base} (KVAR)	3125	3125
V_{base} (V)_{line-line RMS}	450	450
I_{base} (A)_{RMS}	4009	4009
pf	0.8	0.8
Pole Pairs	2	2
H (sec)	2.137	1.7083
r_a (Ω) p.u.	0.00515	0.00618
x_l (Ω) p.u.	0.08	0.096
x_{aq} (Ω) p.u.	1	1.2
r_{kq} (Ω) p.u.	0.0613	0.07356
x_{kql} (Ω) p.u.	0.329787	0.395744
x_{ad} (Ω) p.u.	1.768	2.1216
r_f (Ω) p.u.	0.00111	0.001332
x_f (Ω) p.u.	0.136829	0.164195
r_{kd} (Ω) p.u.	0.023968	0.028762
x_{kdl} (Ω) p.u.	0.333829	0.400595
x_q (Ω) p.u.	1.08	1.296
x_d (Ω) p.u.	1.848	2.2176
x_{kq} (Ω) p.u.	1.3298	1.5957
x_q'' (Ω) p.u.	0.328	0.3936
x_d' (Ω) p.u.	0.207	0.2484
x_d'' (Ω) p.u.	0.172	0.2064
x_f (Ω) p.u.	1.9048	2.2858
x_{kd} (Ω) p.u.	2.1018	2.5222
t_{do}' (sec)	4.7846	4.7846
t_{qo}'' (sec)	0.10081	0.10081
t_{do}'' (sec)	0.048521	0.048521
t_d' (sec)	0.5553	0.5553
t_d'' (sec)	0.038912	0.038911

$$x_q = x_{aq} + x_l$$

$$x_d = x_{ad} + x_l$$

$$x_{kq} = x_{aq} + x_{kql}$$

$$x_q'' = x_l + \frac{x_{aq} * x_{kql}}{x_{kql} + x_{aq}}$$

$$x_d' = x_l + \frac{x_{ad} * x_{fl}}{x_{ad} + x_{fl}}$$

$$x_d'' = \frac{1}{\left(\frac{1}{x_{ad}} + \frac{1}{x_{kdl}} + \frac{1}{x_{fl}}\right)} + x_l$$

$$x_f = x_{ad} + x_{fl}$$

$$x_{kd} = x_{ad} + x_{kdl}$$

$$t_{do}' = \frac{1}{\omega * r_f * x_f} + \frac{1}{\omega * r_{kd} * x_{kd}}$$

$$t_{qo}'' = \frac{x_{kq} + x_{aq}}{\omega * r_{kq}}$$

$$t_{do}'' = \frac{\left(x_{kdl} + \left(\frac{x_{ad} x_{fl}}{x_{ad} + x_{fl}} \right) \right)}{\frac{\omega r_{kd}}{1 + \frac{\frac{x_{kd}}{\omega r_{kd}}}{\frac{x_f}{\omega r_f}}}}$$

$$t_d' = \frac{\left(x_{fl} + \frac{x_{ad} x_l}{x_{ad} + x_l} \right)}{\omega r_f} + \frac{\left(x_{kdl} + \frac{x_{ad} x_l}{x_{ad} + x_l} \right)}{\omega r_{kd}}$$

$$t_d'' = \frac{\left(x_{kdl} + \left(\frac{x_{ad}x_{fl}x_l}{x_{ad}x_{fl} + x_{ad}x_l + x_{fl}x_l} \right) \right)}{\omega r_{kd}} \cdot \frac{\left(x_{kdl} + \left(\frac{x_{ad}x_l}{x_{ad} + x_l} \right) \right)}{\omega r_{kd}} \cdot \frac{1 + \frac{\omega r_{kd}}{\left(x_{fl} + \left(\frac{x_{ad}x_l}{x_{ad} + x_l} \right) \right)}}{\omega r_f}$$